

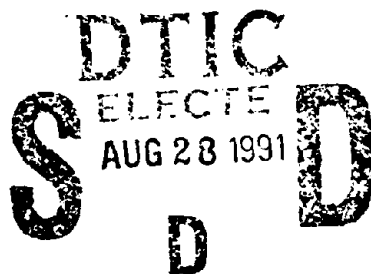
(2)

AN ANALYSIS OF THE FREQUENCY CHARACTERISTICS OF CORONA DISCHARGE AT LOW PRESSURE

AD-A239 940

T. Gregory Lewis
George G. Karady
Murray D. Sirkis

July 1991



Thesis

APPROVED FOR PUBLIC RELEASE; DISTRIBUTION UNLIMITED.



PHILLIPS LABORATORY
Directorate of Advanced Weapons and Survivability
AIR FORCE SYSTEMS COMMAND
KIRTLAND AIR FORCE BASE, NM 87117-6008

01 0 22 094

91-09064

This final report was prepared by the Phillips Laboratory, Kirtland Air Force Base, New Mexico, Job Order 9993LABS. Captain Thomas Gregory Lewis (WSBOF) was the Laboratory Project Officer-in-Charge.

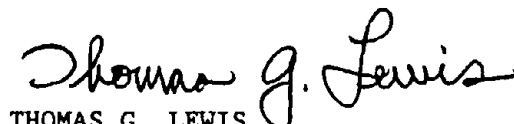
When Government drawings, specifications, or other data are used for any purpose other than in connection with a definitely Government-related procurement, the United States Government incurs no responsibility or any obligation whatsoever. The fact that the Government may have formulated or in any way supplied the said drawings, specifications, or other data, is not to be regarded by implication, or otherwise in any manner construed, as licensing the holder, or any other person or corporation; or as conveying any rights or permission to manufacture, use, or sell any patented invention that may in any way be related thereto.


This report has been authored by an employee of the United States Government. Accordingly, the United States Government retains a nonexclusive, royalty-free license to publish or reproduce the material contained herein, or allow others to do so, for the United States Government purposes.

This report has been reviewed by the Public Affairs Office and is releasable to the National Technical Information Service (NTIS). At NTIS, it will be available to the general public, including foreign nationals.

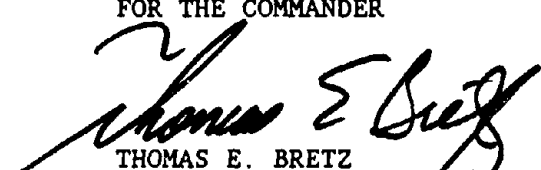
If your address has changed, if you wish to be removed from our mailing list, or if your organization no longer employs the addressee, please notify PL/WSBOF, Kirtland AFB, NM 87117-6008 to help usist.

This report has been reviewed and is approved for publication.


THOMAS G. LEWIS
Captain, USAF
Project Officer


WILLIAM J. BIERCK, JR.
Lieutenant Colonel, USAF
Chief, Test Operations Branch

FOR THE COMMANDER


THOMAS E. BRETZ
Lieutenant Colonel, USAF
Chief, Shock Physics Division

DO NOT RETURN COPIES OF THIS REPORT UNLESS CONTRACTUAL OBLIGATIONS OR NOTICE ON A SPECIFIC DOCUMENT REQUIRES THAT IT BE RETURNED.

REPORT DOCUMENTATION PAGE			Form Approved OMB No. 0704-0188	
Public reporting burden for this collection of information is estimated to average 1 hour per response, including the time for reviewing instructions, searching existing data sources, gathering and maintaining the data needed, and completing and reviewing the collection of information. Send comments regarding this burden estimate or any other aspect of this collection of information, including suggestions for reducing this burden, to Washington Headquarters Services, Directorate for Information Operations and Reports, 1215 Jefferson Davis Highway, Suite 1204, Arlington, VA 22202-4302, and to the Office of Management and Budget, Paperwork Reduction Project (0704-0188), Washington, DC 20503.				
1. AGENCY USE ONLY (Leave blank)	2. REPORT DATE 1991 July	3. REPORT TYPE AND DATES COVERED Thesis; Jan 90 - Apr 91		
4. TITLE AND SUBTITLE AN ANALYSIS OF THE FREQUENCY CHARACTERISTICS OF CORONA DISCHARGE AT LOW PRESSURE		5. FUNDING NUMBERS PR: 9993 TA: LA WU: BS		
6. AUTHOR(S) T. Gregory Lewis, George G. Karady, and Murray D. Sirkis				
7. PERFORMING ORGANIZATION NAME(S) AND ADDRESS(ES) Phillips Laboratory Kirtland AFB, NM 87117-6008		8. PERFORMING ORGANIZATION REPORT NUMBER PL-TR--91-1043		
9. SPONSORING/MONITORING AGENCY NAME(S) AND ADDRESS(ES)		10. SPONSORING/MONITORING AGENCY REPORT NUMBER		
11. SUPPLEMENTARY NOTES				
12a. DISTRIBUTION/AVAILABILITY STATEMENT Approved for public release; distribution unlimited.		12b. DISTRIBUTION CODE		
13. ABSTRACT (Maximum 200 words) Corona discharge is becoming more of a concern now that the space program is looking at higher power and voltage requirements for future missions. Improved detection methods for studying corona discharge will increase the knowledge base of how this phenomenon occurs, what effects it has on power systems, and how it is affected by outside influences. A better understanding of corona discharge will enable designers to improve on the space applications of insulation and dielectrics, and develop proper detection techniques. A test system was designed and constructed to measure the frequency spectrum of corona discharge current in low pressure. Various test samples in different arrangements were energized by ac voltage until corona discharge occurred. This same test was repeated at different pressures. The results indicate that the frequency spectrum of the discharge current changes with a change in pressure. At low pressures, the discharge frequency spectrum is concentrated in a narrow band with a peak at 17 kHz. As the pressure is increased, the spectral width increases to include components across a much broader band. Other tests were performed to correlate the frequency spectrum data to the shape of the discharge pulse and the physical appearance of the glow discharge.				
14. SUBJECT TERMS Corona Low Pressure Partial Discharge		Electrical Discharge Partial Discharge (PD) Detection Frequency Spectrum		15. NUMBER OF PAGES 85
17. SECURITY CLASSIFICATION OF REPORT UNCLASSIFIED		18. SECURITY CLASSIFICATION OF THIS PAGE UNCLASSIFIED		16. PRICE CODE
17. SECURITY CLASSIFICATION OF REPORT UNCLASSIFIED		18. SECURITY CLASSIFICATION OF THIS PAGE UNCLASSIFIED		19. SECURITY CLASSIFICATION OF ABSTRACT UNCLASSIFIED
20. LIMITATION OF ABSTRACT				

For my wife
 Trish
 and the "kidlets"
 Lisa
 Christopher
 Bryan
 and Nathan



Accession For	
NTIS CRA&I	<input checked="" type="checkbox"/>
DTIC TAB	<input type="checkbox"/>
Unannounced	<input type="checkbox"/>
Justification	
By	
Distribution/	
Availability Codes	
Dist	Avail and/or Special
A-1	

CONTENTS

<u>Chapter</u>		<u>Page</u>
1	INTRODUCTION	1
	A. Overview	1
	B. Statement of problem	2
	C. Objective	2
2	BACKGROUND LITERATURE	4
	A. Corona mechanism	4
	B. Previous and current investigations	10
	C. Summary and conclusions	20
3	EXPERIMENTAL PROCEDURE	21
	A. Test setup	21
	B. Procedure	25
	C. Limitations and assumptions	26
4	EXPERIMENTAL RESULTS	28
	A. Physical appearance	28
	B. Pulse capture results	30
	C. Spectrum results	36

CONTENTS (Concluded)

<u>Chapter</u>		<u>Page</u>
5	DATA ANALYSIS AND INTERPRETATION	49
	A. Physical appearance	49
	B. Pulse capture	53
	C. Frequency spectrum	54
6	CONCLUSIONS AND RECOMMENDATIONS	62
	A. Conclusions	62
	B. Recommendations	64
	REFERENCES	66
	APPENDIX: HP 3561A TECHNICAL DATA	70

FIGURES

<u>Figure</u>		<u>Page</u>
1.	Electron avalanche.	4
2.	Voltage-current characteristics of a dc discharge.	7
3.	Space charge distortion.	9
4.	Schematic diagram of corona discharge test circuit.	21
5.	Schematic diagram of corona discharge test circuit for frequency spectrum data.	23
6.	Schematic diagram of corona discharge test circuit for pulse capture.	24
7.	Change in voltage and charge with pressure.	30
8.	Discharge at 6.1 Torr, 478 Volts.	31
9.	Discharge at 6.1 Torr, 526 Volts.	32
10.	Discharge at 7 Torr, 355 Volts.	33
11.	Discharge modes in AC voltage.	34
12.	Corona discharge pulse at 4.6 Torr, 504 Volts.	35
13.	Corona discharge pulse at 6 Torr, 545 Volts.	36
14.	Frequency spectrum at 0.75 Torr, 647 Volts.	37
15.	Frequency spectrum at 0.3 Torr, 506 Volts.	38
16.	Frequency spectrum at 1 Torr, 317 Volts.	39
17.	Frequency spectrum at 2 Torr, 349 Volts.	40
18.	Frequency spectrum at 5.4 Torr, 319 Volts.	40

FIGURES (Concluded)

<u>Figure</u>		<u>Page</u>
19.	Frequency spectrum at 8.5 Torr, 346 Volts.	41
20.	Frequency spectrum at 10 Torr, 390 Volts.	42
21.	Frequency spectrums of 0.075, 2 and 5.4 Torr.	42
22.	Photograph of corona discharge from 10-100 kHz.	44
23.	Photograph of corona discharge frequency spectrum from 10-30 kHz.	44
24.	Frequency spectrum at 0.07 Torr, 635 Volts.	45
25.	Frequency spectrum with pressure held constant.	47
26.	Magnitude of 17 kHz component in corona discharge.	48
27.	Changes in the physical appearance of corona discharge with a change in pressure.	49
28.	Frequency response of the corona test circuit.	54
29.	Paschen curve of CIV for parallel wires.	55
30.	Typical frequency spectrum response.	56
31.	Variation of 17 kHz signal with pressure.	57
32.	Frequency ranges with pressure for -105 dBV	58
33.	Frequency ranges with pressure at -90 dBV.	59
34.	Frequency ranges with pressure for -80 dBV.	60
35.	Detection bands for partial discharge detector.	63

TABLES

<u>Table</u>		<u>Page</u>
1.	Corona discharge variations with pressure.	28

Chapter 1 INTRODUCTION

A. Overview

The phenomenon of corona discharge has been of interest to engineers and scientists for many years. Seamen of old told tales of the glow they called 'St. Elmo's fire' that appeared on the ships' mast when storms approached at night. Pilots report the edges of their wings sometimes glow when flying through thunderclouds [1]. These naturally occurring events have led to a great deal of research and testing in the area of corona discharge and its effects.

The field of high-voltage insulation for transmission lines is a well investigated and studied area. Most utility companies use high-voltage towers and the air to insulate their lines from ground objects. Oils, liquids, gases and other chemicals are also used as insulating mediums.

As space travel becomes more commonplace, the techniques developed by these utility companies to control corona discharge will be looked at for space power applications. However, the vacuum of space and the constraints of spacecraft design will not allow implementation of the insulation techniques used on earth. The issues of weight, size, reliability, and low gravitational fields become very important. The weight and size of liquid or solid insulators must be limited since "excess" in weight or size could not be supported for spaceflight. Low gravitational fields may cause bubbling in liquid dielectrics. Reliability in insulation systems is needed due to the prohibitive cost and difficulty of repairs in space.

B. Statement of problem

As the requirements for space power systems increase, higher voltage levels and higher operating frequencies will be required. These higher values, needed to reduce the size and weight of equipment (transformers, capacitors, wiring, etc.), will approach powers near megawatts and voltages up to hundreds of kilovolts [2]. At these high voltages, a proper understanding of corona discharge under low pressure conditions becomes very important. The next generation of space craft will operate at altitudes in the range from 24,000 to 46,000 meters, which corresponds to a pressure range of about 20 to 1 Torr [3]. Corona discharge could be a serious problem in their power systems and associated cabling. Deterioration and eventual breakdown of the dielectric can cause serious problems for space applications. Research performed at Arizona State University has shown that the breakdown voltage decreases with the decreasing separation distance between a wire and a ground plate. This lower breakdown voltage will manifest itself as partial discharge (PD) in the voids of the solid insulating material, electromagnetic disturbances, reduced flashover voltage, and deterioration of the insulating material which may eventually lead to breakdown. Due to the high altitude at which these space craft will be operating, low pressure may result in severe corona discharge problems.

C. Objective

In order to avoid problems with corona discharge, a better understanding of the actual phenomenon at low pressures is needed. As corona discharge is better understood, special requirements for design and operation can be drafted for use in

making high altitude spacecraft operational. This thesis will investigate the frequency spectrum of the discharge current and relate the change in the spectrum to other discharge phenomena as a function of pressure. Three different areas will be examined. First, a study of the physical appearance of corona discharge will be made as a function of pressure. Second, a study of the pulse shape of the corona discharge as a function of pressure will be explored, and third, by examining the frequency components of the corona discharge current, a study of the change in the frequency spectrum of the discharge current will be examined as a function of pressure. A better understanding of the corona discharge will aid in the development of the power systems for space craft of the future and help to avoid the problems associated with low pressure (high altitude) discharge. A more complete understanding of corona discharge will aid in the development and use of more precise detection equipment.

Chapter 2 BACKGROUND LITERATURE

A. Corona mechanism

The basic mechanism involved in the corona discharge occurs as a series of steps. Free electrons are present in gas and act as the starting point of corona discharge. When a sufficient overvoltage is applied to the test setup, the free electrons, triggered by the resulting electric field are accelerated through the gas in which they reside. Some of these electrons acquire enough energy so that when they collide with other atoms, more electrons are released as a result. This produces an avalanche effect as shown in Figure 1 below.

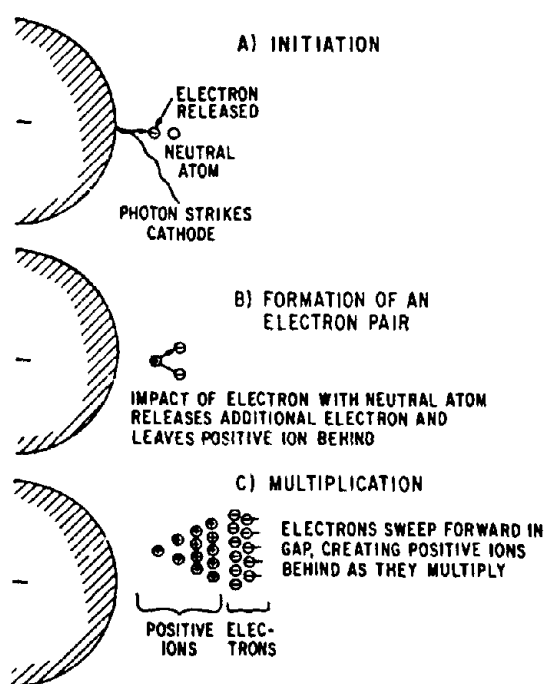


Figure 1. Electron avalanche. Copyright © 1987. Electric Power Research

Institute. EPRI EL-2500. Transmission Line Reference Book: 345 KV and Above. Second Edition. Reprinted with permission.

Many of the collisions that take place are elastic in that the electron loses very little of its kinetic energy. When an electron has sufficient energy to strike an atom and cause excitation, the atom jumps to a higher energy state. The electron(s) of the atom shift to a higher state, and as they return to their former state emit energy in the form of light (visible corona) and electromagnetic waves.

The 'corona avalanche' produces millions of positive and negative ions. The entire process occurs in a microsecond time frame. Tests show [4] that the entire process is probabilistic in nature. The size of the collision volume, materials used and pressure all play a very important role in the development of corona discharge. An electron in a gas at a pressure of 1 Torr and 0 degrees centigrade makes only 10 to 100 collisions for each centimeter it travels. As the pressure increases, the number of atoms per cubic centimeter increases, as does the probability of a collision.

Townsend developed a coefficient to describe the number of electrons that were produced from a single electron traveling in a uniform electric field over a distance of 1 cm. Known as Townsend's first ionization constant, the discharge current in the avalanche of electrons can be described as

$$I = I_0 e^{\alpha d}$$

where alpha is Townsend's first ionization coefficient and d is the gap distance. I is the gap current and I_0 is the initial current in the gap due to outside sources.

As an electric field stresses a gap in air, the free electrons migrate toward the grounded wire and create a very minute current. As the field increases, secondary processes which were also studied by Townsend come into play [5]. When the

secondary processes are included, the equation above can be more accurately written as

$$I = I_0 \frac{e^{\alpha d}}{1 - \gamma(e^{\alpha d} - 1)}$$

where gamma, Townsend's second ionization coefficient, represents the secondary processes that contribute to the discharge current. If the denominator approaches zero, the current will become infinite. This is the case when

$$\gamma(e^{\alpha d} - 1) = 1$$

and according to the studies done by Townsend [6], this is the condition which defines the onset of the corona discharge. The Townsend criterion expresses the condition in which an avalanche, starting from a negative electrode, can be self-sustaining. Meek and Craggs [7] examined the Townsend criterion and made the following observations:

(a) when the value on the left of the equal sign above is less than 1, the discharge current is not self-maintained. This means that if no initial current is in the gap due to outside or external sources, the current ceases.

(b) when the value on the left is equal to 1, the discharge is self-sustaining and can continue without the need of the external source.

(c) when the value on the left is greater than 1, the ionization produced by successive avalanches is cumulative.

In low pressure corona discharge, a large number of phenomena may occur. If we look at the voltage-current characteristics of a parallel plate arrangement with dc voltage source we have a curve of the type shown in Fig. 2. Each electron that leaves the cathode moves toward the anode producing ionization on the way. The positive ions produced drift toward the cathode, producing more electrons by

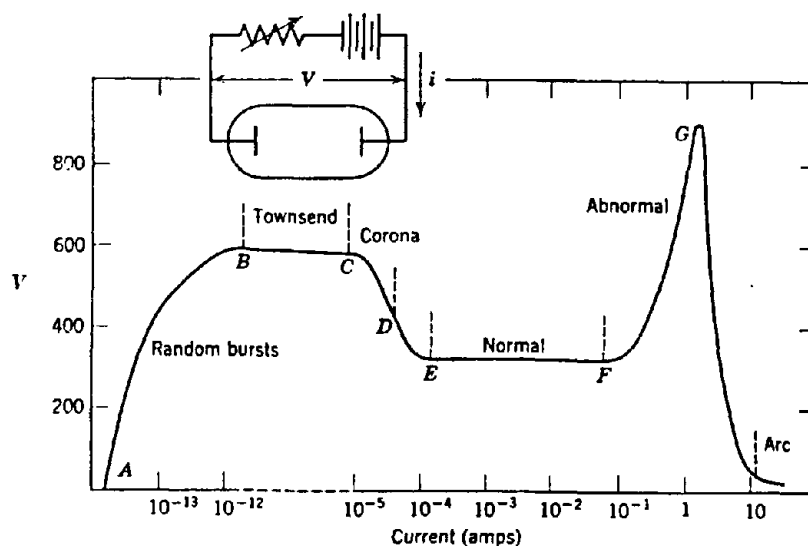


Figure 2. Voltage-current characteristics of a dc discharge. Copyright © 1966.

Introduction to Electrical Discharges in Gases, S.C. Brown. Reprinted by permission of John Wiley & Sons, Inc.

secondary emission when they hit the cathode. At very low voltages and currents, the multiplication is insufficient to lead to a self-sustaining discharge and the current occurs in random bursts. If a supply of electrons is provided by a photoelectric source, the current is controlled by the intensity of the illumination. Breakdown occurs at the beginning of what is called the Townsend discharge region, BC . As the

current increases from C to E , the discharge begins to glow visibly and the potential across the tube drops to a constant value. This is the region which has been called "corona discharge" [8]. The region in which the potential difference is constant, EF , is called the "normal glow". Here the discharge covers only a part of the cathode, the area covered increasing with the current. The current density remains constant. When the whole cathode is covered with glow, increasing the current further causes the voltage to rise; this is the region FG called the abnormal glow. The high-current operation of the discharge is termed the arc. Most of the early work in discharges centered around the study of the visual behavior of the corona discharge, and led to the classifications of the different regions that were visible.

EPRI [4] points out that the Townsend breakdown criterion, while being conceptually useful, is not used because the discharge process is much more complicated than the equation implies. For example, the effect of space charge is not taken into account. Space charge will disrupt the uniformity of the electric field in a parallel plate arrangement. The ions and electrons that are produced in the discharge will move at different rates; the electrons move much faster than the ions. In an arrangement with a cathode and anode, the ions will accumulate on the cathode in a much higher concentration than the electrons on the anode. This results in an ion concentration at the cathode that greatly exceeds the electron concentration at the anode. As mentioned before, this space charge affects the electric field, E , according to Poisson's equation [9] shown below.

$$\epsilon \frac{\partial E}{\partial x} = -\rho$$

Here ρ is the net charge density and x is the separation distance between the two electrodes. The general form of the distortion of the E-field can be seen as shown in the Figure below.

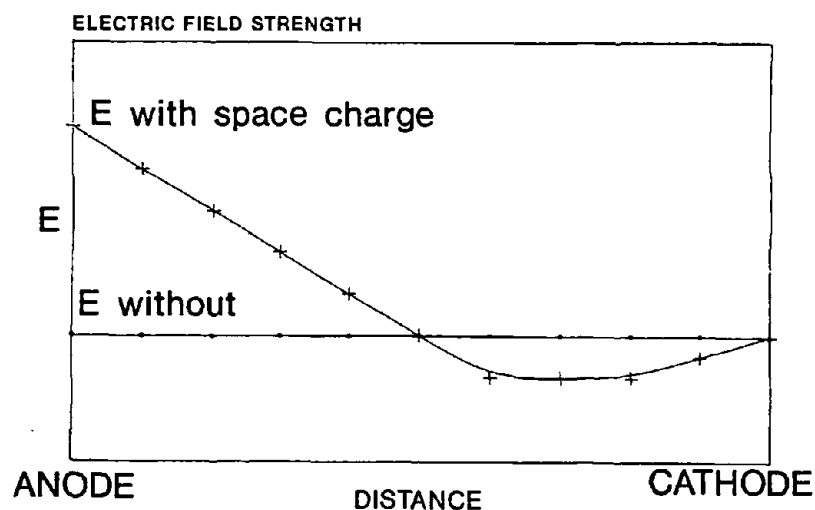


Figure 3. Space charge distortion.

This is shown as a generalization only since the actual shape of the field intensity depends on the variation of ρ with x . The constant line in the figure indicates the E-field for ρ equal to 0. Vuhuu and Comsa [10] calculated the electric field, E_{sp} , created by a space charge left from the occurrence of an avalanche. This is given by

$$E_{sp} = \frac{eN}{4\pi\epsilon_0 r_D^2}$$

where N is the number of positive ions, and r_D is the radius. Epsilon is the permittivity of the vacuum and e is the charge of a positive ion (1.6×10^{-19} coulombs).

Substitution of these constants permits this equation to be rewritten in a more simplified form as

$$E_{sp} = 1.5 \times 10^{-17} \frac{N}{r_D^2}$$

where the units are volts per centimeter.

B. Previous and current investigations

Some of the earliest work in gaseous conduction was described by Gilbert in his 'de Magnete' in 1600. Later studies made by Coulomb in 1785 [1]. With the development of adequate vacuum capabilities, research in corona discharge made a quantum leap forward with the work of Friedrich Paschen in 1889 [11]. The curves which now bear his name, have become a cornerstone in corona studies. He found that the voltage required for corona inception varied with pressure and distance. His law states that at a given potential difference, the field being uniform, the product of the pressure at which the discharge occurs and the distance between the electrodes will be constant. Stated differently, as the product diminishes the discharge potential decreases until, at a critical value, it becomes a minimum for a given gas. For still smaller values of the product, the sparking potential increases rapidly.

The effect of high altitudes on aircraft insulation was discussed by Berberich *et al.* [12] in 1944. His paper presents a large number of break down voltages versus altitude or air density measurements and concludes that the breakdown strength of rod gaps is lower than for uniform field conditions. However, the differences in breakdown voltages around the Paschen curve minimum are negligible. The first

publication on corona problems in aircraft was presented by Wilson [13] in 1944. He described the problems and offered design methods to avoid corona. Pendleton [14] proposed applying semiconducting coatings on ceramic bushings to increase the corona inception voltage. Linder and Steele [15] showed that the corona inception voltage decreases as the operating voltage frequency increases. For example, the inception voltage at the Paschen minimum is 230 volts at 60 Hz, 160 volts at 299 Khz, and 50 volts at 1 GHz. In 1962, Starr [16] proposed design methods for avoiding flashover in a space environment. He noted that a thin silicon rubber coating would greatly increase the corona inception voltage. However, barriers suspended between the electrodes proved to be even more effective than the silicon coating. In 1971, Paul and Burrowbridge [17] presented methods for preventing electrical breakdown in space. Their methods included the avoidance of high electric fields and the avoidance of critical gas pressures. Selection of materials, scrupulous cleanliness, good mechanical design, solid potting or complete venting, and frequent testing were found to be the major requirements to success. In 1972, NASA [18] collected all aerospace-related corona literature up to that time. Also, in 1984, the Department of Energy [19] collected all data on electrical breakdown in gases. This collection included experimental and theoretical data on sparking potentials, breakdown voltages, corona inception voltages, critical fields, voltage-time characteristics, dielectric strengths and breakdown probabilities.

The phenomena of breakdown has been shown to be dependent on the strength of the electric field. Peek worked to describe this relationship empirically. Gary *et al.* [20] described Peek's law as

$$E_c = E_0 \delta \left(1 + \frac{K}{\sqrt{\delta R}} \right)$$

where E_c is the critical field, or ionization threshold of the corona inception voltage in kV per cm. Delta is the relative air density given as a ratio of the air pressure in Torr and the air temperature in centigrade (it is equal to 1 at 760 Torr and 25 degrees centigrade). R is the wire radius (cm), and K is a constant equal to 0.038. E_0 is also a constant with a value of 31 kV per cm.

Chong-hui and Zheng-xiang [21] proposed a modification to calculate the corona inception voltage at high altitudes. They developed a modification of Peek's formula for calculating the corona inception voltage at six different altitudes;

$$E_c = 31.5 \delta K_h \times \left(1 + \frac{0.305}{\sqrt{\delta R}} \right)$$

where they used a constant of

$$K_h = 1 + 6.12 \times 10^{-3} (H - 11)$$

where R is the inner conductors radius (cm), delta is the relative air density at the six different altitudes and H is the absolute humidity and K_h is the absolute humidity

factor. They proposed including the absolute humidity into the equation as shown above. Their work was focused on transmission lines and the six variations of height over mountainous terrain compared to flat land.

A number of papers have been written on the effects of the frequency of the voltage source has on corona discharge. He and Hall [22] studied the frequency and pressure dependence of RF discharge excited CO₂ waveguide lasers. They found that the output of the laser is strongly dependent on the frequency of excitation. At the optimum excitation frequency of 125 MHz, 30.6 W at 12 percent efficiency and 0.83 W/cm was achieved.

Suganomata *et al.* [23] studied the variations of light emissions from a parallel plate discharge at frequencies of 100 and 500 kHz. Their results suggest that the plasma in the gap between the two electrodes becomes an electron source to sustain the discharge by detaching electrons from negative ions. Sato and Haydon [24] studied the onset and development of corona under RF conditions in a point-to-plane arrangement in air and N₂ from 80 Torr to 760 Torr at 10 MHz. Using an image intensifier system they were able to make time-resolved observations of the initiation of corona as well as the intermittent and continuous breakdown phenomena. They determined that the pressure and geometrical arrangement of the test setup can greatly affect the appearance of the corona discharge.

Ishikawa *et al.* [25] built a planar diode system to produce a discharge in SF₆ at a pressure of 0.2 Torr with a driving frequency of 30 kHz to detect negative ions. They examined the negative ion density on the order of 10⁸ cm⁻³.

Damas and Robiscoe [26] worked on the development of detection methods of RF signals emitted by an arc discharge. They analyzed the arc radiation signals detected by a typical RF receiver operating at a set frequency and bandwidth. They determined that the RF receivers respond to the derivative of the arc current rather than the current itself. However, at low frequencies, suitable information can be obtained because the size of the time constant of the current pulse can be correlated with the strength of the receiver input signal. Measurements at high frequencies require considerable correction for instrumental settings and do not provide direct information regarding the arc. Seeboeck and Koehler [27] investigated the temporal intensity modulation of spectral lines for a parallel plate arrangement in Argon gas. By the use of a sapphire window and fiber optic cable they could examine the optical spectrum of the discharge. They found that the spectral lines were very much determined by the pressure and developed a simple model to correlate their experimental findings with their theoretical results.

A few papers that examined very briefly the frequency characteristics of the discharge itself have been published. In 1933, Ballantine [28] studied the effect of fluctuation noise due to ions formed by collision in electronic amplifier tubes at various pressures. While his work was not directly involved with corona discharge, what he did find is rather interesting. At pressures of the order of 10^{-4} mm in mercury vapor a decrease in the noise at the higher frequencies was observed. However, in argon the noise was uniform throughout. With mercury vapor at higher

pressures (4×10^{-3} Torr) the noise spectrum became peaked with the frequencies of the peaks depending on the electron current flowing in the amplifier tube.

In 1976, Ishikawa and Suganomata [29] studied the frequency shift of the voltage oscillation of the positive column in a SF_6 gas discharge. They used an external voltage applied to the anode (80 volts peak to peak) and 2 kV applied to the cathode of two parallel plate aluminum electrodes spaced 15 cm apart. By increasing the external anode voltage once the corona discharge had begun, the frequency of the discharge pulses would increase at specific points. The authors concluded the phenomenon may be ascribed to the motion of negative ion clouds in the SF_6 gas discharge. In 1984 [30], they published another paper on the frequency of ionization waves in SF_6 gas. Again, they used aluminum plate electrodes, 2.2 cm in diameter and spaced 60 cm apart. They studied the pressure range from 0.5 to 1.1 Torr and the current range 0.1 to 0.3 mA. They determined that two modes of ionization waves exist. Mode I waves showed that the frequency changes from 20 to 80 kHz with an increase in the discharge current. The Mode II wave was a 1 kHz wave with a group velocity less than 2×10^{-3} cm/s, which changed from a forward wave to a backward wave with an increase in the discharge current. They concluded that the Mode I wave was induced by positive ions and Mode II by heavy negative ions. A later paper [31] discussed the existence of half-integer (subharmonics) in the ionization waves in SF_6 gas. The same set-up was used as before, and they determined that the half-harmonic excitation depends on the applied frequency and voltage.

In 1984, Sato and Haydon [32] used a spectrometer to analyze the spectroscopic information obtained from the corona discharge. They used a plane-to-toroidal gap of 15 mm at pressures of 80, 200, 650 Torr. The intensities of the spectral line emissions with relation to the gap length for both air and nitrogen were studied. They looked at only the 100 ns period of a single period of RF voltage amplitude at 10 MHz, and noted the change in the spectral line emissions while varying the gas and pressure. Using a point-to-plane arrangement, they found that there was a very distinct polarity effect caused by the ac voltage. With negative polarity on the needle electrode the luminosity in the gap was more extensive than for positive polarity. The luminosity around the needle point was less intense and broadened for the negative polarity than for the positive polarity. They found that the appearance of the luminosity of the corona discharge depends not only on the voltage and polarity but also on the conditions in the gap such as electron and ion distributions produced prior to the event. This observation supports the statement made above about the effect of space charge.

Ogle and Woolsey [33] investigated point-to-plane corona discharges in SF_6 for currents up to 20 mA. They used a pressure range of 0.1 to 10 Torr. They found that as the pressure increased, the appearance of the discharge changed from an abnormal glow with a diffuse positive column to a normal glow with a constricted positive column. Another interesting study of the corona discharge appearance and its change with voltage and distance was that done by Vuhuu and Comsa [10]. Using a point-to plane configuration, they used thick (greater than 1.6 mm) and thin (less

than 1.6 mm) wires at various gap lengths and applied a voltage across the gap until discharge started. The voltage was then increased and the changes were noted. As an example, the discharge sequence for a thick wire is as shown below.

For short gaps.....burst pulses

glow

sparkover

For medium gaps.....burst pulses

burst pulses which may

or may not cause

sparkover

if the previous streamers

do not cause sparkover,

occurrence of glow

sparkover

For long gaps.....burst pulses

glow

sparkover

From this we see the appearance of the streamers depends not only on wire size but also on gap distance. The gap distance was varied to a maximum of 20 cm. The terms "short", "medium" and "long" relate to 20 cm.

In 1988, Suganomata *et al.* [34] looked at the typical waveforms of the discharge current in CF_4 , SF_6 and N_2 gases. They again used parallel plate aluminum electrodes, and found that the waveforms varied depending on the gas medium used. In SF_6 , a current pulse before the main discharge current was seen at about a quarter of the period after the zero voltage phase. The current pulse is due to electron detachment from negative ions. In N_2 , there was no detachment current pulse, but a pulsed current was observed just after the zero voltage level. They ascribed this current pulse to electrons being accelerated in the afterglow plasma produced by the discharge during the preceding half-period. The CF_4 discharge current was much more complicated than the other two. The electron current pulse appears just after the zero voltage phase, and is accompanied by an oscillation of a few cycles with a frequency of about 2 MHz. The oscillation is believed to be caused by a current-driven instability due to the dissociative electron attachments in the gas. Beyer *et al.* [35] investigated the possibilities of acoustic partial discharge detection on cast-epoxy resin dry-type transformers. They measured the frequency spectrum of acoustic PD signals to determine what range would be needed for sonic sensors. They did not investigate the spectrum at different pressures or voltages.

The statistical properties of corona pulses have been studied previously using pulse-height analysis (PHA) for discharges in SF_6 and various mixtures of SF_6 in N_2 and water vapor [36-38]. PHA has also been used to study the discharge characteristics inside insulating cavities and other equipment [39]. These studies were all done at atmospheric pressure, however. Al-Arainy *et al.* [40] used a

multichannel analyzer to study the variation of AC corona pulse amplitudes in a point-to-plane configuration at atmospheric pressure. They found that for AC corona near the corona inception voltage, in a point-to-plane arrangement, the pulse amplitudes follow a Gaussian type of probability distribution. However, when the applied voltage is progressively increased, the deviation from a Gaussian type of probability distribution also increased.

Malik and Al-Arainy [41] studied the electromagnetic interference (EMI) caused by corona and gap discharges on high-voltage transmission and distribution lines in the desert of Saudi Arabia. They measured the EMI frequency spectrum at different points on 33 kV transmission lines. These results, used in conjunction with measurements of the lateral profile (EMI deviation vs. distance) and statistical variations of the lines, were used to compare television interference of the desert with more wet climates.

Cross [42] studied the current in a point-to-plane corona discharge using a fast storage oscilloscope. He found that the current increased when a porous layer was present on the plane during the discharge. This was due to an increase in the frequency of the Trichel pulses at the cathode and very little (less than 0.1 %) can be attributed to activity at the anode. It was proposed that the increase in the Trichel pulse frequency is caused by neutralization of the negative ion space charge by positive ions produced by discharges in the porous layer.

Bandel [43] studied the point-to-plane corona in dry air for various pressures and point sizes. He looked at the physical steps in the development of the discharge by monitoring the voltage and pressure and noting when burst pulse, streamer and steady corona onset occurred. He found that the process is heavily dependent on pressure.

C. Summary and conclusions

An extensive literature search revealed that while much has been done to examine corona discharge, no research has been done to examine the frequency spectrum of the discharge current. While there has been a great deal of testing to examine the effect of source frequency on corona discharge, there has been no investigation into the frequency components of the corona discharge itself, and what changes occur with a corresponding change in pressure. The current literature concludes that the nature of the corona discharge depends on the pressure and operating frequency of the voltage in use.

This thesis will examine how the frequency components of the corona discharge current vary with pressure. The frequency spectra will be related to the shapes of individual pulses (captured with a digital oscilloscope) and the physical appearance of the corona discharge at different pressures.

Two parallel copper wires will be used. This arrangement was chosen for ease of setup and less contamination of the sample. Wires were readily available and could be changed out quickly and easily if they were damaged or considered too dirty or oily. This ensured repeatable results when the tests were conducted.

Chapter 3 EXPERIMENTAL PROCEDURE

A. Test setup

Three different tests were run to collect data for this thesis. The three different test setups will be shown. In the first test, the voltage, current, and charge of the corona discharge were measured, and its physical appearance was recorded as the pressure was varied. The test arrangement for this is shown in Figure 4 below.

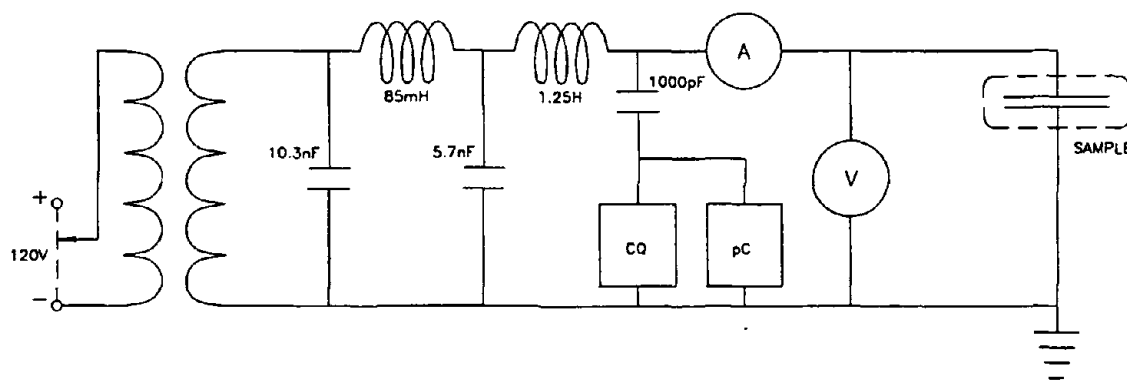


Figure 4. Schematic diagram of corona discharge test circuit for charge, voltage and current data.

The samples consisted of bare copper wires arranged in a parallel configuration inside a glass vacuum chamber specially designed and constructed for these tests. The chamber consisted of an outgassing port and two ports for vacuum gauges used to

monitor the pressure in the chamber. Care was taken to keep the chamber free from dirt and oils by minimizing hand contact. A vacuum pump with a control valve was used to control the pressure in the chamber. This pressure was monitored by two different low pressure gauges, one digital and one analog to ensure accuracy. Room air was used as the gas in the tube. The wires were carefully arranged inside the chamber at various separation distances with care taken to ensure that the wires were straight and free from nicks and abrasions that might interfere with the measurements.

Most commercially available PD detectors are designed and calibrated for testing either commercial high-voltage cable or machinery, or for evaluating of small samples of insulating gases, liquids, and solid materials at AC frequencies from 50 Hz to 400 Hz, as well as DC. During testing, these detectors are usually directly coupled to the test article by direct electrical connections. Modifications and specialized high-voltage connections were required for operating in the vacuum chamber [44]. As shown in Figure 4, a high-voltage transformer was connected to the system and controlled by a 60 Hz variable transformer. The transformer was connected to a high-voltage filter to remove any 60 Hz supply generated high-frequency noise and increase the transformer high-frequency impedance. The high-voltage input was connected to one of the wires in the vacuum chamber, while the other wire was grounded. The measurements were taken through a coupling capacitor as shown in Figure 4, rated at 1000 pF. This is one of many different methods which may be used for corona detection. It is fast, and very reliable. The use of a coupling

capacitor, which falls under the 'electronic pickup' category, facilitates measurement of the high-frequency voltage and current impulses created by the corona discharges. The relative signal sensitivity is excellent, and the small size and simple design of the apparatus make it an ideal method for corona discharge detection. Bilodeau *et al.* [44] indicate that the coupling capacitor method exhibits an instantaneous signal response time, and is sensitive to neither external light nor external pressure. The signal is then taken from the coupling capacitor to the coupling quadripole. This coupling quadripole is used as a transmission element between the detector and the coupling capacitor. It splits the measurement signal into a partial discharge signal and a voltage signal. Both of these signals are then fed into a Haefely 561 partial discharge detector.

In the second test the frequency spectrum of the corona discharge current was studied. The test arrangement is shown in Figure 5 below.

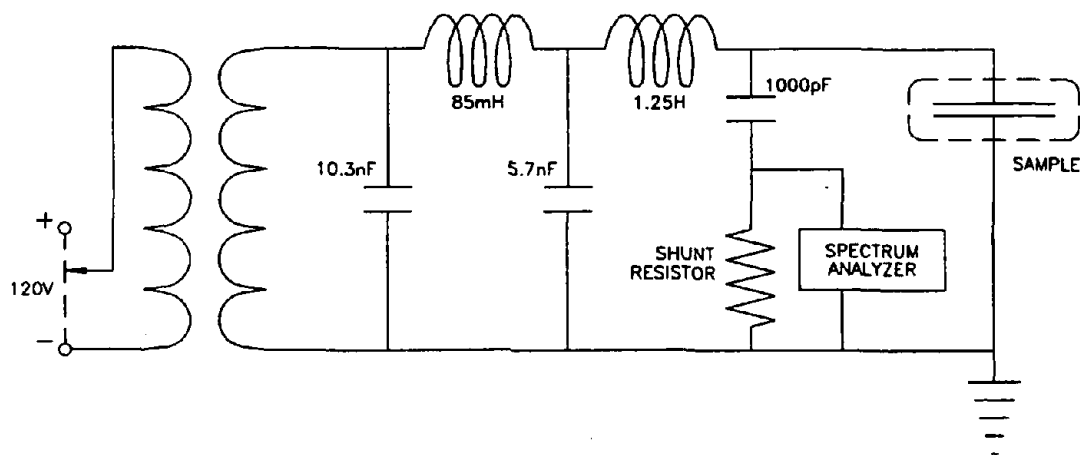


Figure 5. Schematic diagram of corona discharge test circuit for frequency spectrum data.

A shunt resistor was used to catch the signal for a Hewlett Packard 3561A dynamic signal analyzer. The high voltage filter and transformer setup remained unchanged. This setup will record the frequency spectrum of the discharge when the discharge occurs. In the third test, a fast digital storage oscilloscope was connected to the test sample to capture the shape of the discharge pulse so its dependence on pressure and voltage could be studied. The test arrangement is shown in Figure 6 below. Again, the high-voltage filter and transformer setup was utilized for this test.

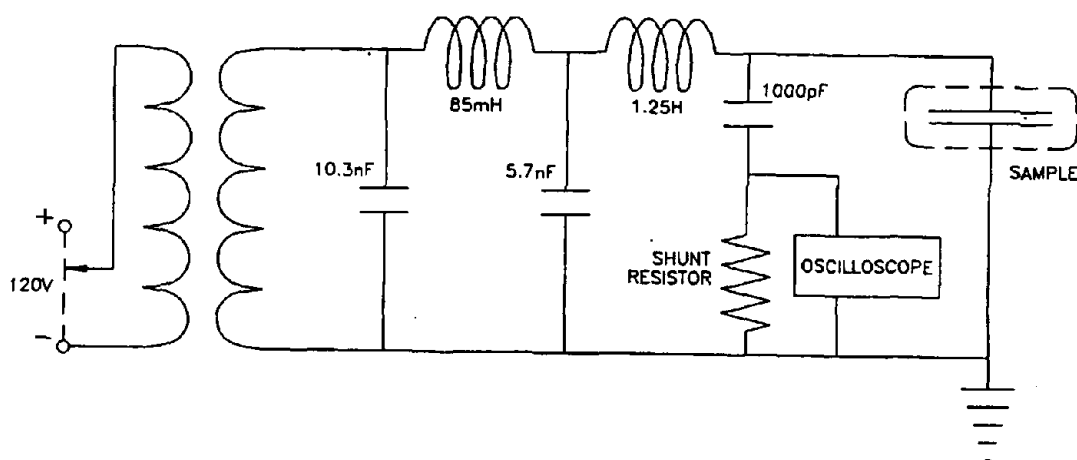


Figure 6. Schematic diagram of corona discharge test circuit for pulse capture.

With the same test configuration and samples, consistency of testing and comparison of the test data is possible.

B. Procedure

Even though three different tests were run, the test procedures were essentially the same. The test sample was placed in the vacuum chamber and the pressure was reduced. An hour was allowed for outgassing before a 60 Hz AC voltage was applied. The pressure was set and held constant as the voltage was slowly increased until corona discharge was detected by either a visual appearance of the corona discharge or an indication by the PD detector. The voltage was then recorded and subsequently was reduced to zero. At least 30 minutes elapsed before the next measurement was taken to allow time for any space charge that might have developed to dissipate. The pressure was then set again and the process was repeated. These procedures were repeated several times over many days to insure reliable data.

The prescribed procedure required a great deal of skill and patience. Great care had to be taken to ensure that the corona discharge was taking place on the test sample and not on the connections or in the circuitry of the filter. As mentioned previously, cleanliness of the chamber and the wires was very important. Any contamination could drastically effect the results of the measurements. Great pains were taken to make each measurement under the same conditions. Outgassing has proven itself to be a concern in these tests. Different gases can enter a vacuum chamber through a number of different ways; backstreaming from the pump, permeation through the walls of the chamber, diffusion from the chamber, desorption

and vaporization from the chamber walls, leaks in the seals or penetrations through the chamber and from the sample or high-voltage putty of the sample in the chamber. Tests have shown that for low pressures, using clean materials in a chamber with negligible leaks, diffusion of gas out of the sample materials dominates from a few hours to a number of years [2]. With this in mind, I decided to outgas for 1 hour for each test, after making sure that each sample was degreased and clean before starting the test. This provided the continuity needed to obtain consistently reliable results.

C. Limitations and assumptions

A few variables were beyond my control in conducting these tests. As mentioned before, the gas used in the chamber was simply room air. No tests were made to determine the composition or humidity of the air as the tests were taken. Some of the tests were performed in the morning, some in the afternoon, and some very late in the evening. However, the temperature of the room air was recorded and the variation was slight between succeeding tests. The highest temperature under which tests were conducted was 22.2 degrees centigrade. The lowest temperature was 21.7 degrees centigrade. It is assumed that this variation does not critically affect the results of these tests. It is further assumed that the room air was constant in its composition over the many days that these tests were taken.

It was also assumed that the wires were completely straight and parallel with each other, and no nicks or cuts caused a localized high field region to affect the corona inception voltage.

While it appears that outgassing is a constant problem in low pressure or vacuum testing, I have assumed that outgassing for 1 hour is sufficient to allow a consistent and reliable, repeatable test.

Chapter 4 EXPERIMENTAL RESULTS

A. Physical appearance

Table 1. Corona discharge variations with pressure.

#	Torr	V	I	pC	APPEARANCE
1	0.06 Torr	667 V	0.14 mA	2 pC	Diffuse, light purple glow inside the entire glass chamber.
2	0.2 Torr	310 V	0.23 mA	0.8 pC	Diffuse, purple glow with a thin pink layer concentrated around the wires.
3	0.5 Torr	315 V	0.75 mA	2.7 pC	Deeper purple glow concentrated around wires, dark space between
4	1 Torr	333 V	2.98 mA	6.2 pC	Two distinct layers around each wire, dark space larger, deeper purple with thin pink layer.
5	3 Torr	605 V	42.0 mA	12 pC	Only one concentrated light purple layer around each wire.
6	5 Torr	708 V	153 mA	36 pC	Violet around each wire with red streamers between.

For the Table above, the results of three different tests were examined. The first test consisted of looking at the physical appearance of the discharge as a function of the pressure while measuring the voltage and current as well as the charge in picoCoulombs. Two wires were placed in a parallel arrangement with a separation distance of 4.8 cm. The test sequence was repeated four different times over a three day period to ensure reliable results. A few items conclusions may be drawn from these tests. The same discharge mechanisms of the parallel wires hold for the parallel plate arrangements. That is, the Crookes dark spot is independent of the arrangement. As described by Loeb [45], the Crookes dark space in the parallel wire arrangement extends outward as the pressure decreases. However, in this case, we see that the dark space becomes more pronounced as the pressure increases. The pink thin layer around the wire is characteristic of the tests run by Brown [8]. He called this the 'first cathode layer' and described it as a pink layer when it occurred in air.

The results show that the intensity of the pC charge is proportional to the voltage. This follows from the equation for the relationship between voltage and charge,

$$q = C \times V$$

where V is the voltage, q is the charge in picoCoulombs and C is the capacitance of the parallel wire arrangement. We must make an assumption on the equation.

We assume that for the parallel wire arrangement the capacitance is constant. The change in the charge with pressure is shown in Figure 7 below.

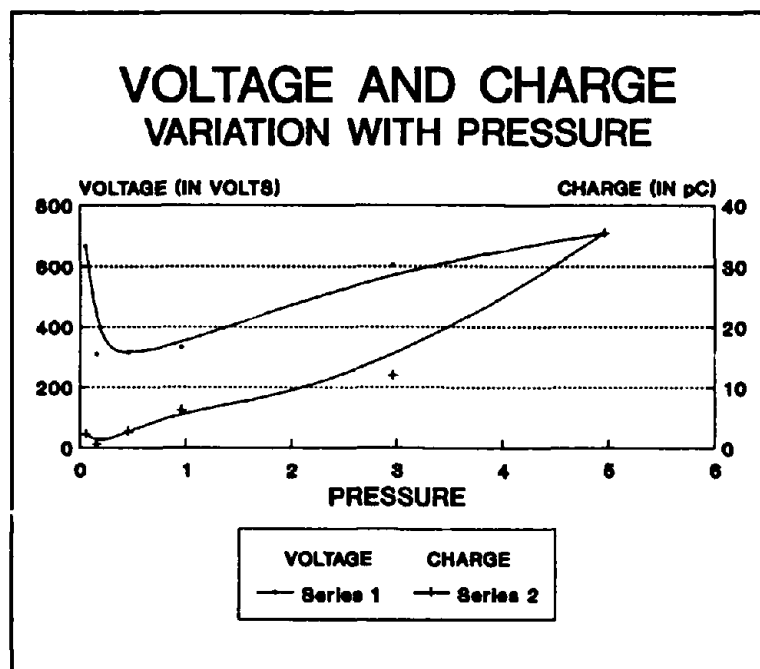


Figure 7. Change in voltage and charge with pressure.

Here we see a correlation between the voltage and the charge of the corona discharge. The current increases nearly linearly with pressure. The six points from Table 1 were plotted on the graph and a curve fitting program was used to connect the points in a 'best fit' curve.

B. Pulse capture results

The shape of the corona discharge pulse as a function of pressure was also examined. A digital storage oscilloscope was connected to the system shown in

Figure 6 to capture the corona discharge. The results of these tests, which were recorded with an HP plotter, are included below.

In Figure 8, we see the results of the corona discharge at 6.1 Torr and 478 Volts.

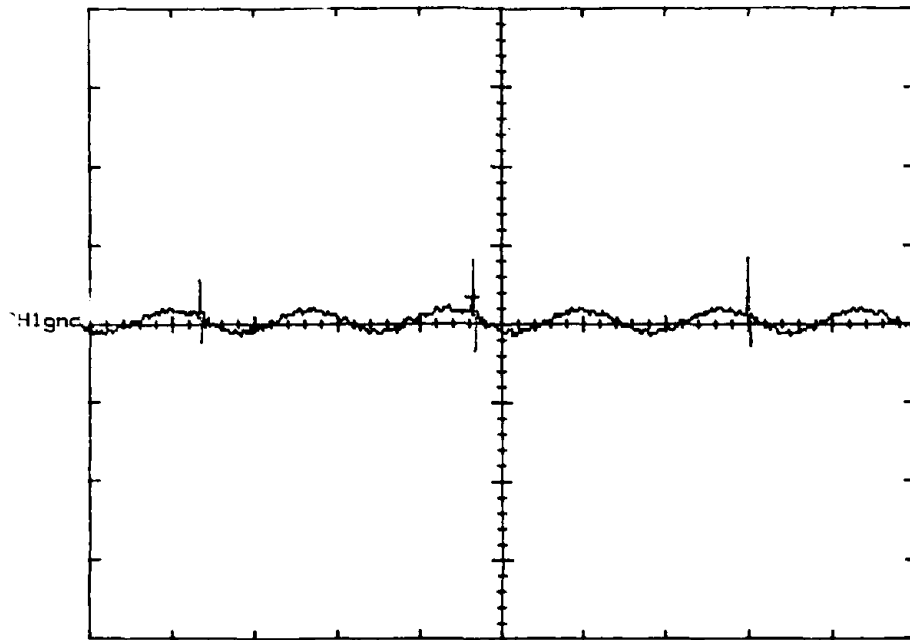


Figure 8. Discharge at 6.1 Torr, 478 Volts.

The 60 Hz sinusoidal wave is from the voltage source and has been greatly magnified to show its relation to the corona discharge pulses. We see from the plot that the discharge is occurring once every 2 periods. In Figure 9, the pressure is still 6.1 Torr, but the voltage has been increased to 526 Volts. In this case we see that the discharge is occurring once every period.

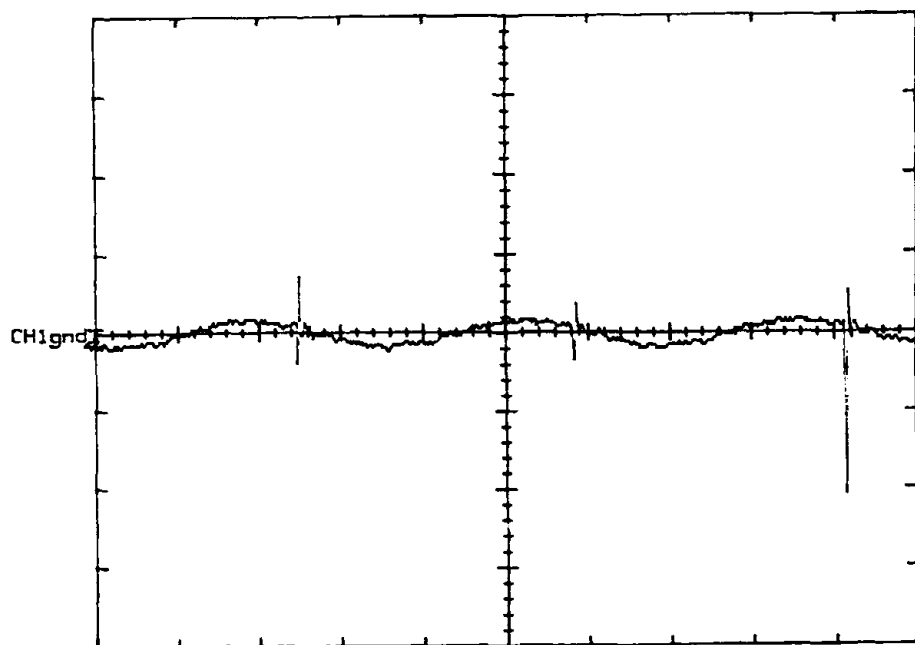


Figure 9. Discharge at 6.1 Torr, 526 Volts.

In other tests, we were able to vary the voltage and get discharges from once every fourth period, every third period and then as shown, every second or every period. Once the voltage has been increased beyond the CIV, discharge occurs with greater frequency.

The plot shown in Figure 10, shows the discharge at 7.0 Torr and 355 Volts. Here we see that just at the CIV, we have a discharge every half period.

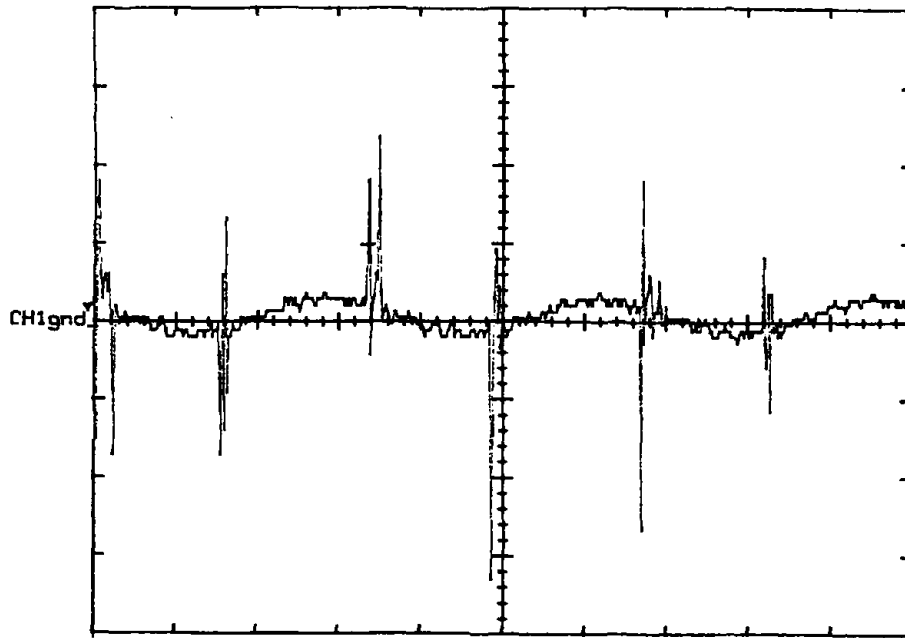


Figure 10. Discharge at 7 Torr, 355 Volts.

From these plots we see that the repetition of the discharge seems to be dependant on both the voltage and the pressure. EPRI [4] has done work in this area, and these results are in substantial agreement with theirs. In Figure 11 below, we see the possible corona modes that can exist with an AC voltage. Space charge may have a very dramatic effect on the type and intensity of the corona discharge. The space charge produced during one half cycle may alter the corona produced on the next half cycle.

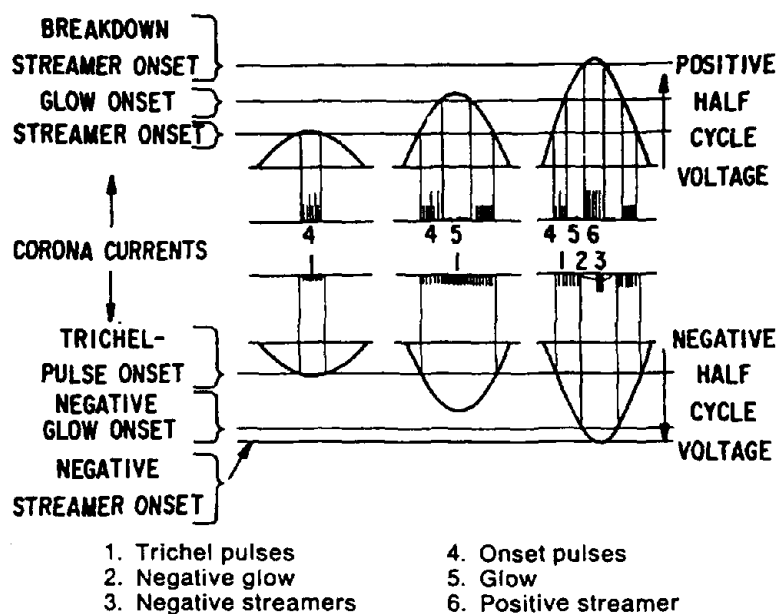


Figure 11. Discharge modes in AC voltage.

The shape of an individual discharge pulse was examined using the same test arrangement as was used for Figures 8, 9, and 10. The fast storage oscilloscope was set to capture a single pulse of the corona discharge current right at the corona inception voltage. As shown in Figure 12, the pulse occurred at a pressure of 4.6 Torr and 504 volts. With the time scale set at 1 microsecond per division, the rise time is shown to be about 0.7 microseconds. In Figure 13, the pressure was increased to 6 Torr, and the pulse was captured when the voltage was increased to 545 volts. The time scale for this figure is now 500 nanoseconds per division. From this we see that the rise time is about 550 nanoseconds. This and other tests indicate that the rise time of the pulse is dependent on the pressure at which the corona discharge occurs.

At low pressures, the rise time was longer than at higher pressures. This indicates that at higher pressures, a fast rise time shows that higher frequency components are present in the discharge.

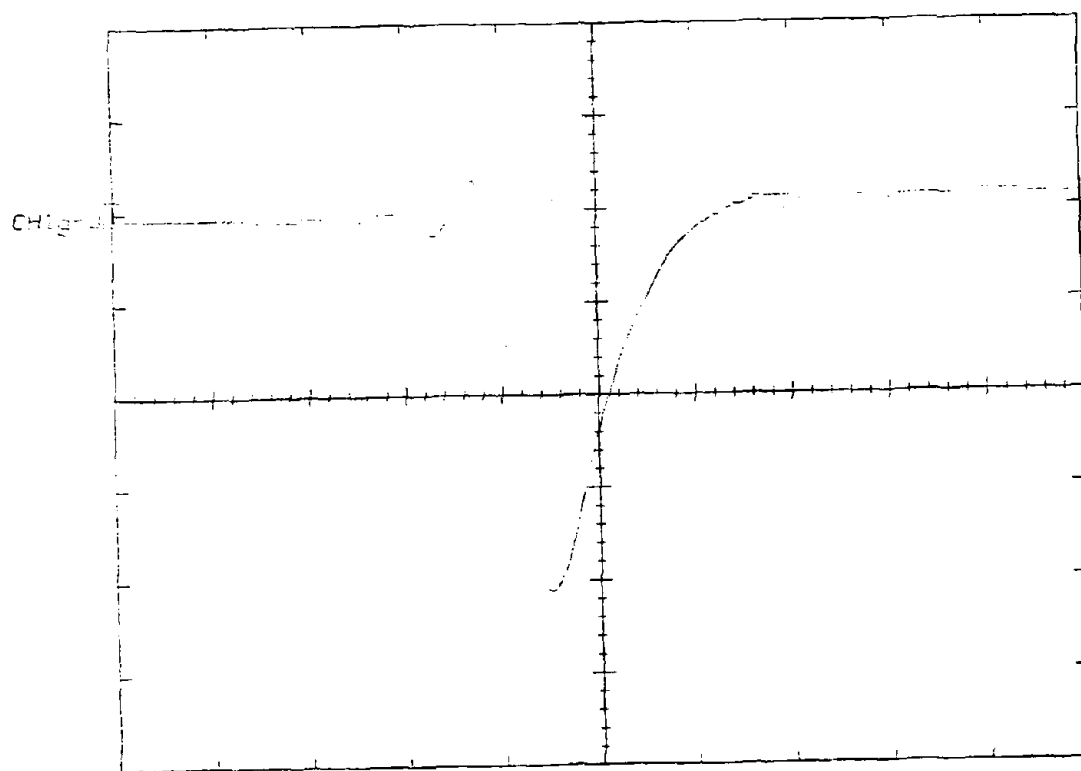


Figure 12. Corona discharge pulse at 4.6 Torr, 504 Volts.

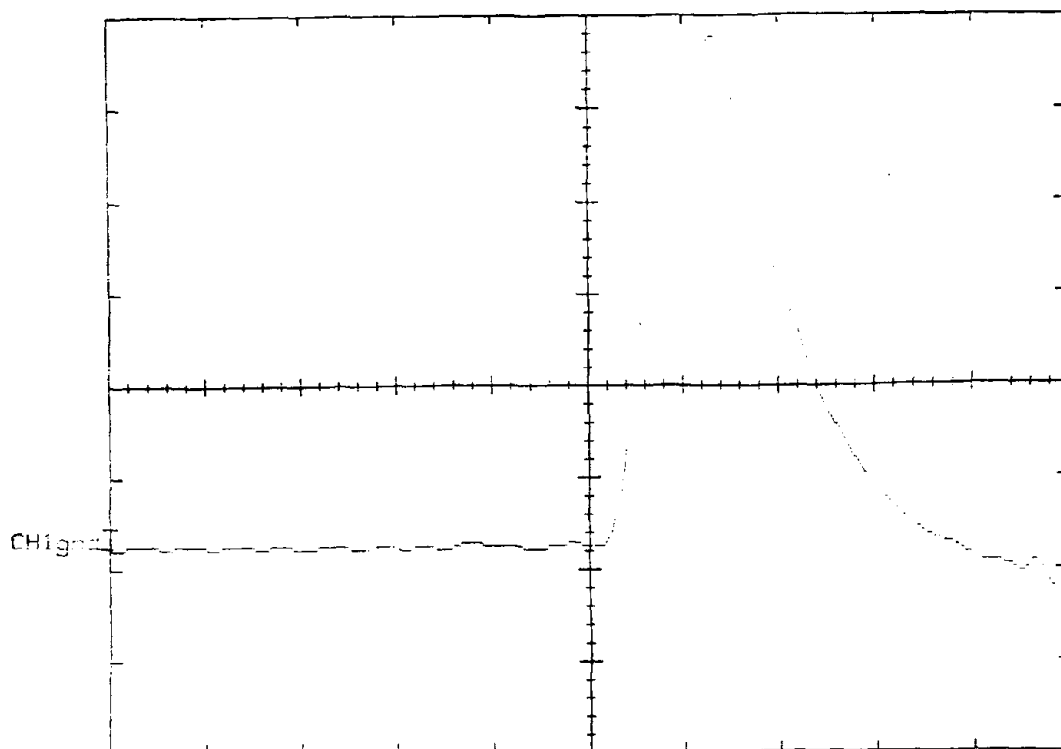


Figure 13. Corona discharge pulse at 6 Torr, 545 Volts.

C. Spectrum results

Finally, a frequency spectrum analyzer was used to display and record the frequency components of the corona discharge as a function of the pressure. The results will be examined in two parts. First, the frequency spectrum will be examined as a function of pressure; and second, the frequency spectrum will be examined as a function of voltage.

These results were obtained using the setup shown in Figure 5. It consisted of two No. 16 gauge solid copper wires with a separation distance of 4.8 cm. As explained in the procedures, the test chamber was evacuated and the pressure was set. The voltage was then increased until the onset of corona discharge.

In the figure below, the frequency spectrum of the corona discharge at the corona inception voltage of 647 V is shown. The pressure was .075 Torr. A small component in the area of 17 kHz is visible.

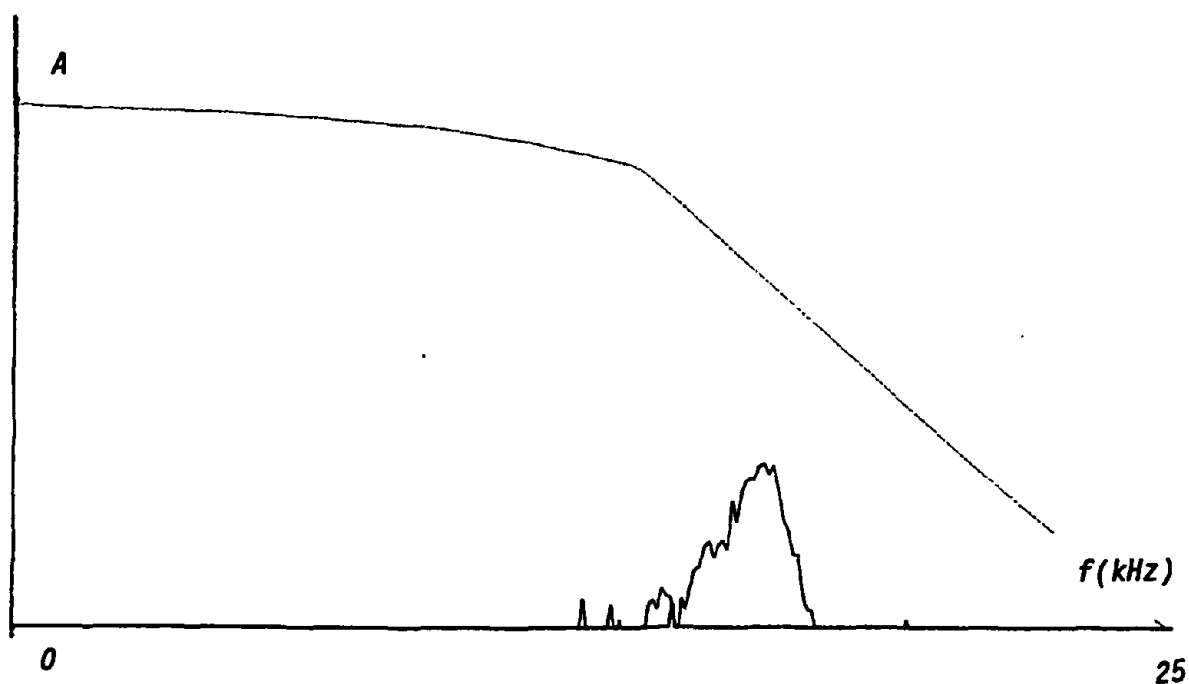


Figure 14. Frequency spectrum at 0.75 Torr, 647 Volts.

The horizontal axis shows the frequency from 0 to 25 kHz and the vertical axis is the relative magnitude of the corona discharge voltage (and current since measurements are taken through a resistor).

In Figure 15 below, the spectrum for a pressure of 0.3 Torr at 506 V is displayed.

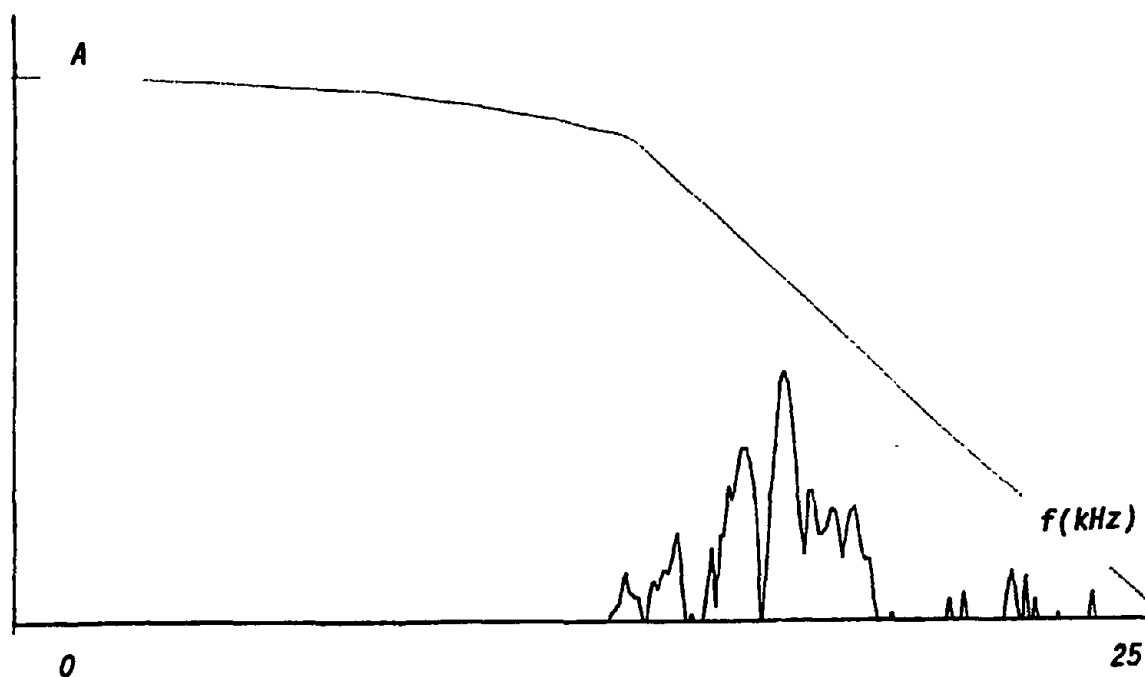


Figure 15. Frequency spectrum at 0.3 Torr, 506 Volts.

Here again, the frequency spectrum of the discharge is centered around 17 kHz, but a broader band of frequencies is included.

In the next figure, the pressure was increased to 1 Torr and corona inception occurred at 317 V. We now see components appearing at very low frequencies and

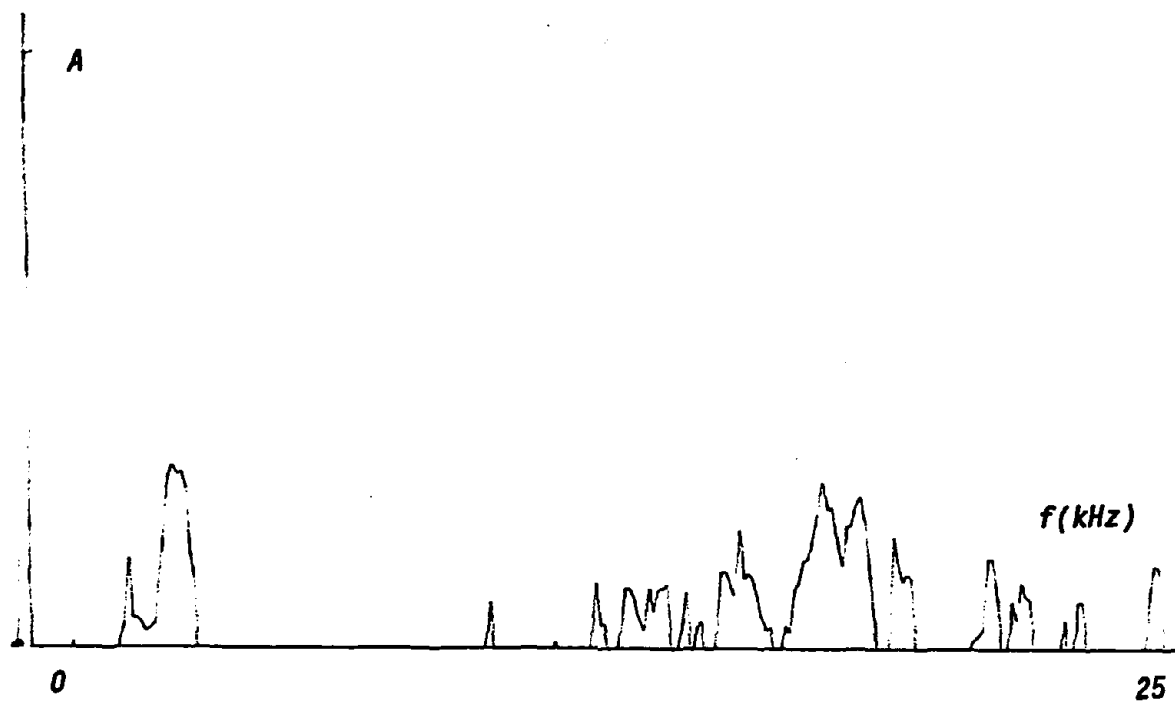


Figure 16. Frequency spectrum at 1 Torr, 317 Volts.

more components from about 11 kHz up to the upper limit of the spectrum analyzer, 25 kHz.

With the pressure increased to 2 Torr, the CIV occurred at 349 V. The spectrum appeared as shown in Figure 17 below. Here a small component appears below about 5 kHz and components exist at almost all frequencies above about 11 kHz. Most frequency components are still nominally centered around 17 kHz.

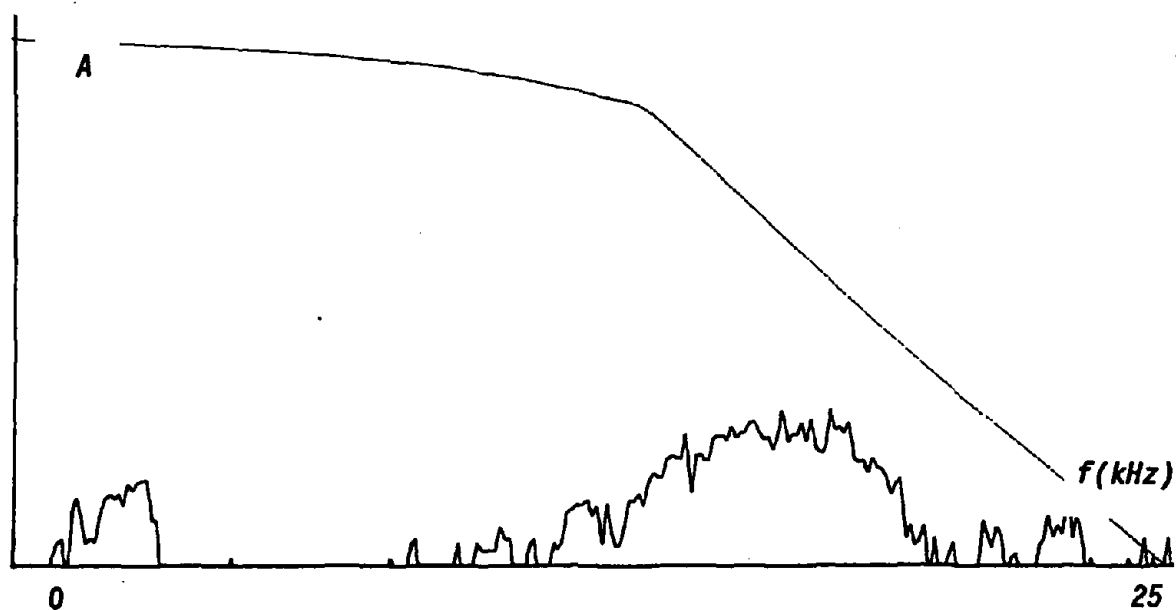


Figure 17. Frequency spectrum at 2 Torr, 349 Volts.

The pressure was next set at 5.4 Torr and discharge occurred at 319 V. In this case a major change in the frequency spectrum was observed. The magnitude of the

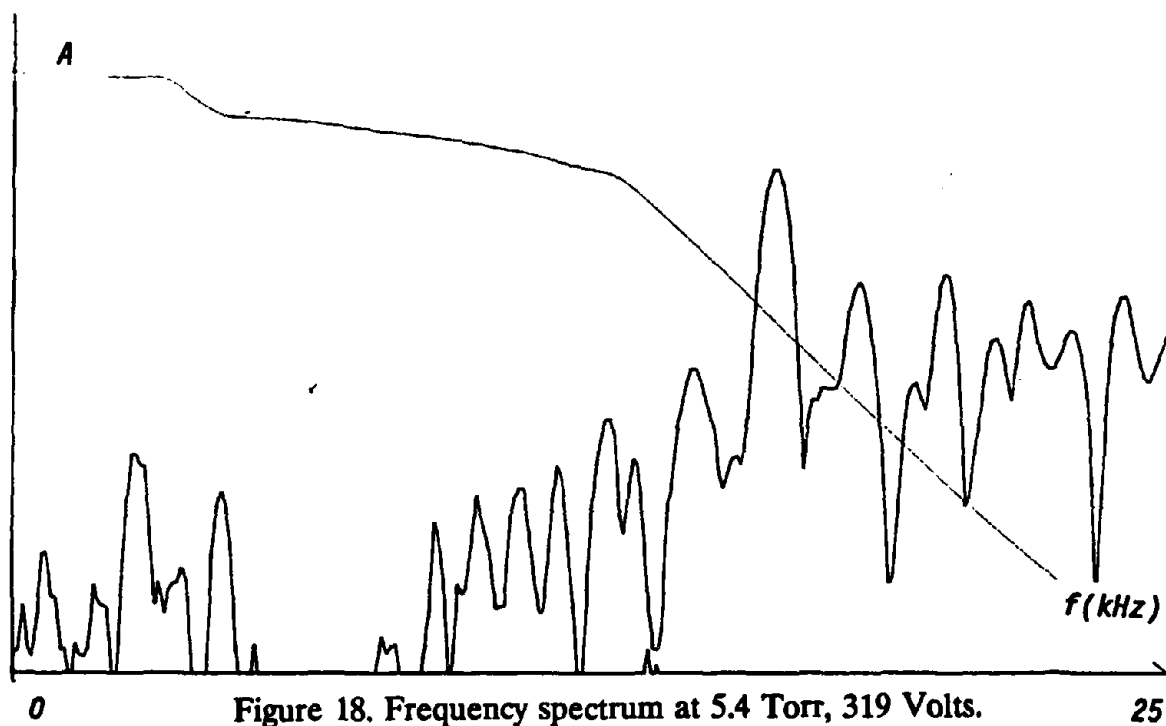


Figure 18. Frequency spectrum at 5.4 Torr, 319 Volts.

discharge has increased drastically. There are still two divisions in the signal. Lower frequency components below 5 kHz and those above about 8 kHz. In addition, there is activity beyond the upper limit of the spectrum analyzer (25 kHz).

When the pressure was increased to 8.5 Torr, the CIV occurred at 346 V. As shown below, the corresponding spectrum is now almost continuous with frequency components across the entire frequency band.

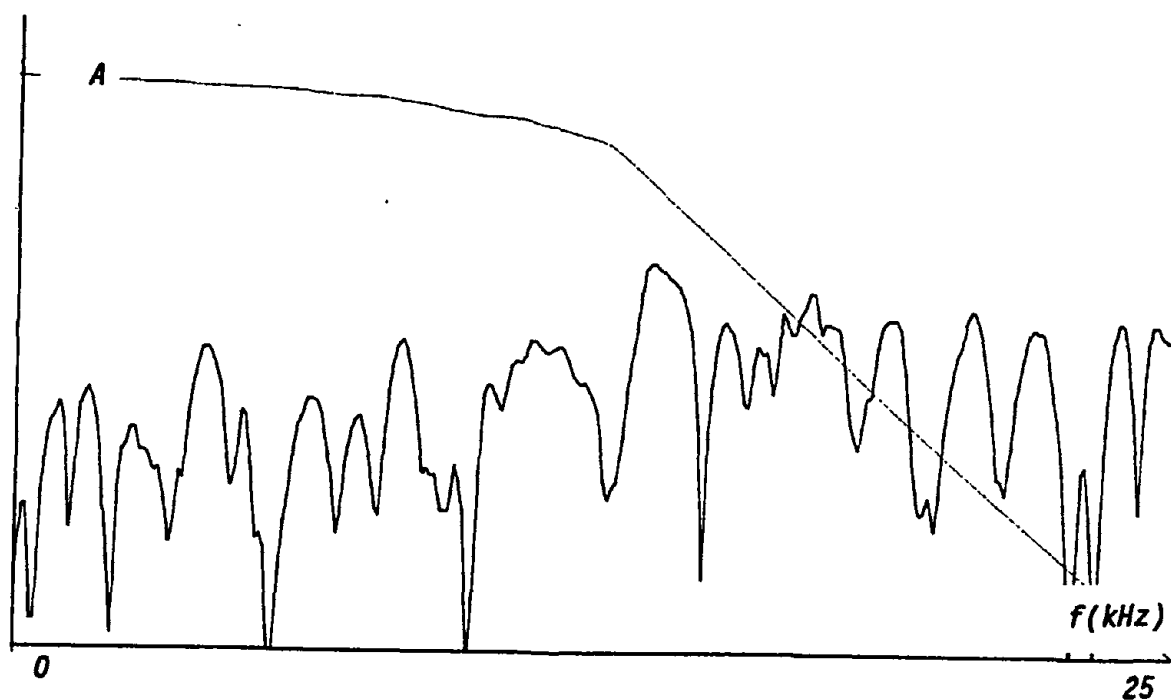


Figure 19. Frequency spectrum at 8.5 Torr, 346 Volts.

There continues to be activity beyond the 25 kHz limit, and based on these data, one could assume a great deal is occurring.

Finally, the pressure was increased to 10 Torr and corona discharge occurred at 390 Volts. As shown below, the magnitude of the frequency components have

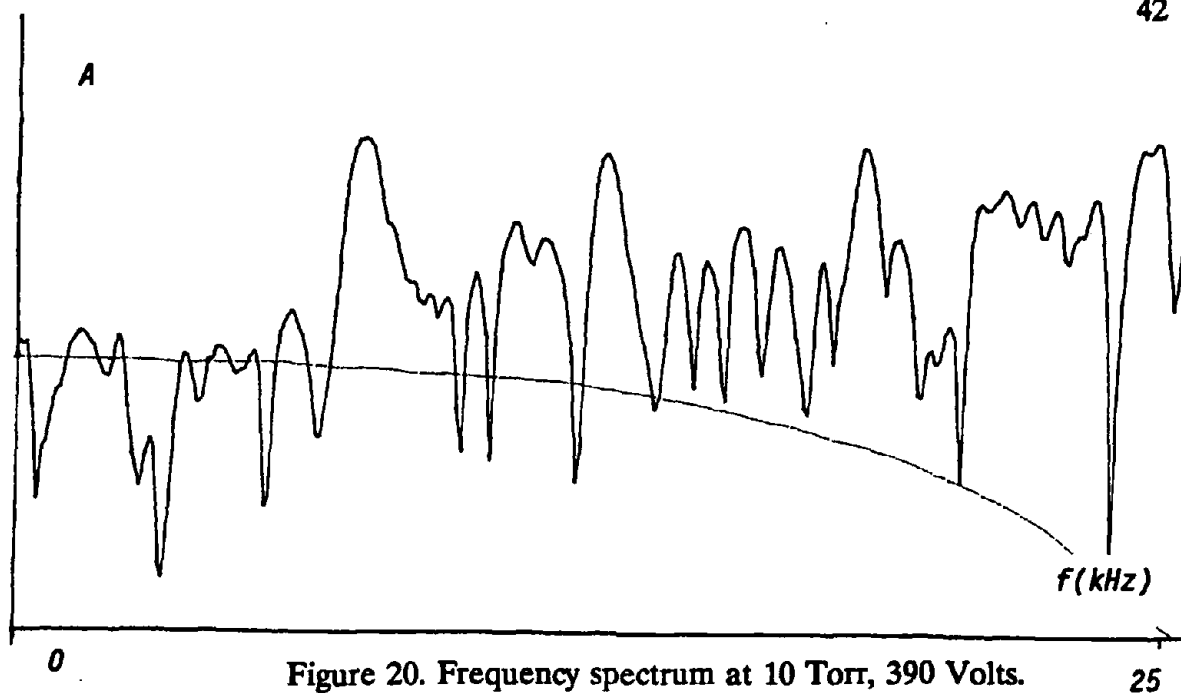


Figure 20. Frequency spectrum at 10 Torr, 390 Volts.

increased at nearly all frequencies of the spectrum.

In order to show the relative change of the frequency spectrum, the spectra for .075, 2 and 10 Torr may be overlaid as shown in Figure 21.

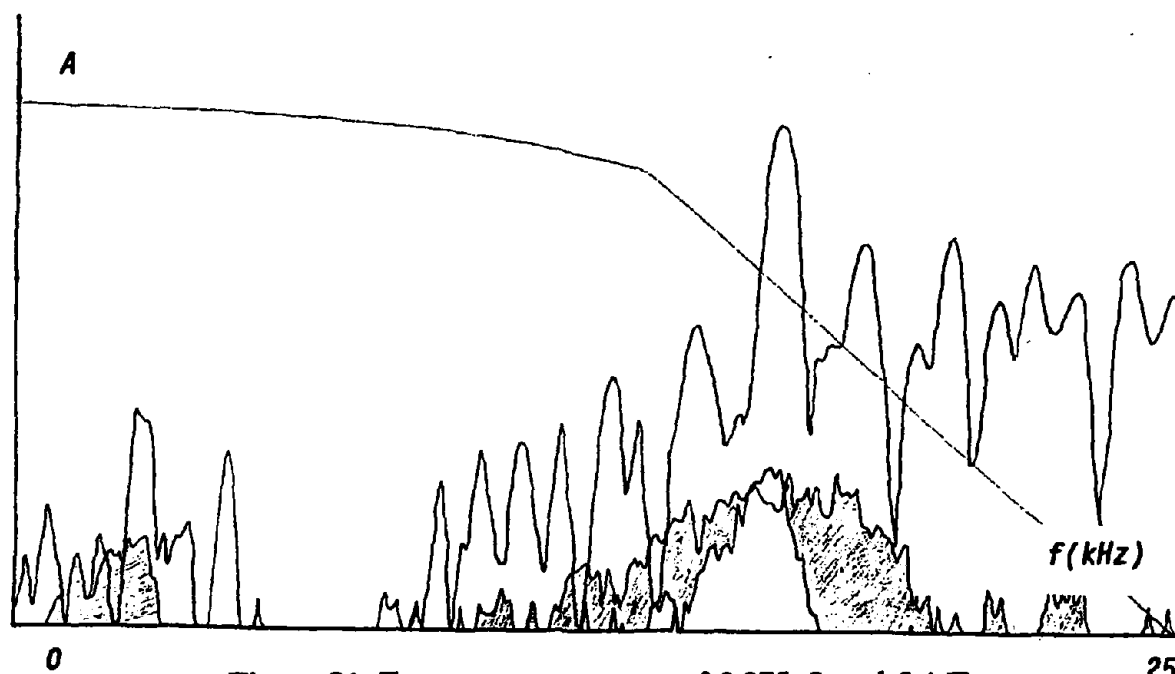


Figure 21. Frequency spectrums of 0.075, 2 and 5.4 Torr.

The dramatic change in the spectrum as a function of pressure is clearly visible. The magnitude and spread of the frequency components are directly related to the pressure in the vacuum chamber.

Since a great deal of activity takes place beyond 25 kHz, it is necessary to study a broader frequency band. A Tektronix 2710 spectrum analyzer was used to examine the spectrum from 10 kHz to 1800 MHz. The components near 17 kHz that appeared in the previous tests, could be displayed as well as those at much higher frequencies.

The setup shown in Figure 5 was used. However, a sample consisting of No. 12 gauge parallel bare copper wires were used. These wires were separated by a distance of 7.5 cm. The test was conducted to determine the frequency components of the corona discharge in a range from 10 kHz to 1800 kHz. The pressure was set at 0.22 Torr, and the voltage was increased. At 300 V, the spectrum consisted of only a signal centered around 17 kHz. There were no other frequency component signals present at higher frequencies. In the photograph below (Figure 22), the range was changed to cover the frequencies from 10 kHz to 100 kHz. The bottom trace is the noise reference level and superimposed on top of that is the corona discharge signal. Other than the components near 17 kHz, no other frequencies were detected.

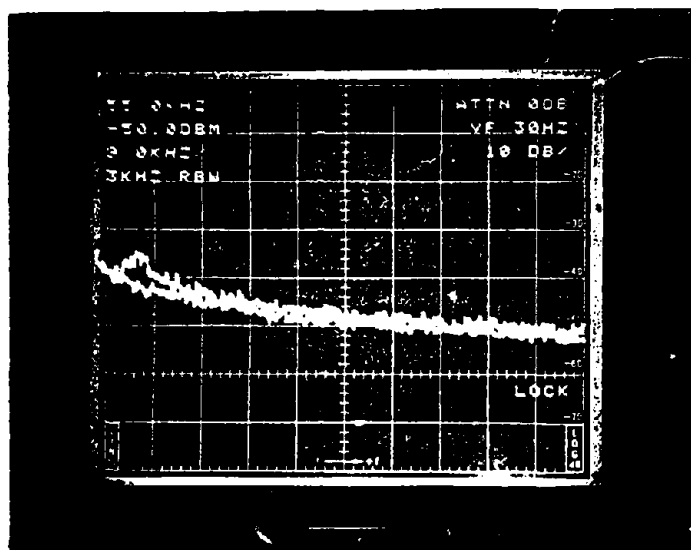


Figure 22. Photograph of corona discharge from 10-100 kHz.

The photo below shows the same setup, pressure and voltage for the range from 10 kHz to 30 kHz.

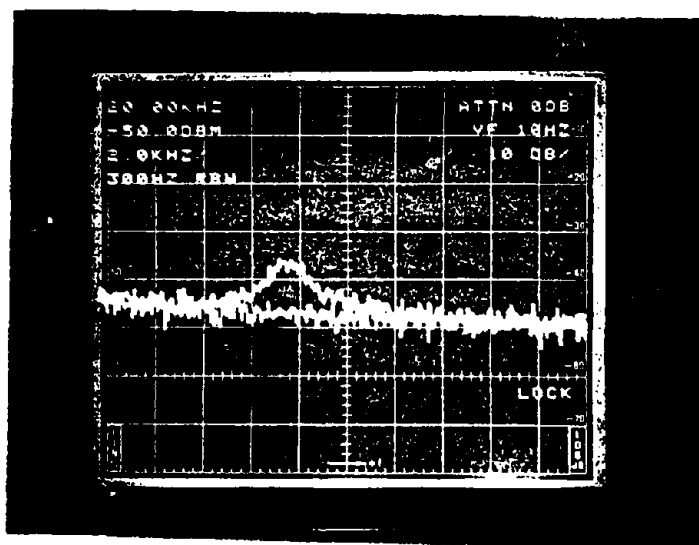


Figure 23. Photograph of corona discharge frequency spectrum from 10-30 kHz.

The bottom trace is again the noise reference level and the upper trace is the corona discharge signal. Here again, only components centered around 17 kHz are seen.

For the remainder of the tests, a Hewlett-Packard 3561A dynamic signal analyzer was used. This equipment has a frequency range of 0 to 100 kHz. Based on the information obtained from the Tektronix analyzer, this machine is adequate for the measurements I had to perform, i.e., majority of the signals fell below 100 kHz.

The technical data on the H-P 3561A is included in Appendix A. This equipment was able to quantify the magnitudes of the corona discharge. The values could be measured in dBV or mVrms. Both display modes were used. The first results are presented next.

The setup consisted of the arrangement as shown in Figure 5 with a sample arrangement of two parallel bare copper wires (No. 12 gauge) with a separation distance of 7.5 cm. A plotter was connected to the Hewlett-Packard Interface Bus (HP-IB) to obtain a hard copy of the display. A sample of this output is given below.

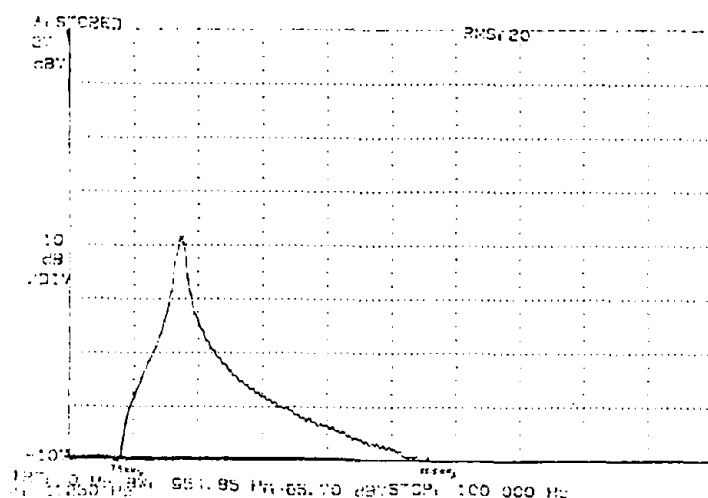


Figure 24. Frequency spectrum at 0.07 Torr, 635 Volts.

Here we see the results of the corona discharge spectrum from 0 to 100 kHz at a pressure of 0.07 Torr just at the CIV of 635 V. We see a peak at 17.25 kHz with a value of -65.7 dBV. The cutoff is at 55.5 kHz with a value of -107 dBV. The measurement range for the 3561A is +27 to -120 dBV noise floor (22.4 Vrms to 1 microV noise floor). The greater sensitivity of this apparatus explains the high frequency "tail" in Figure 24 that was not apparent on the previous figures.

In second part of this analysis, the frequency spectrum of the corona discharge is examined when the pressure is left constant. The voltage is increased past the corona inception voltage until complete breakdown occurs.

For this series of tests, the setup of Fig. 5 was used with two parallel No. 12 gauge bare copper wires spaced 7.5 cm apart. The pressure was set at 5.8 Torr and CIV occurred at 481 V. The voltage was then increased to 755 Volts (pressure kept at 5.8 Torr) and the spectrum was taken. Finally, the voltage was increased to 927 Volts and the spectrum was taken. The results of these three tests are superimposed in Figure 25 below.

The data show that even though the magnitude of the discharge current increases, the frequency spectrum of the corona discharge does not change. This means, there are no new frequency components which appear in the discharge. Even though we saw the repetition of the discharges increase with the voltage in the section on pulse capture, we see that the frequency spectrum of the corona discharge does not increase with an increase in the voltage.

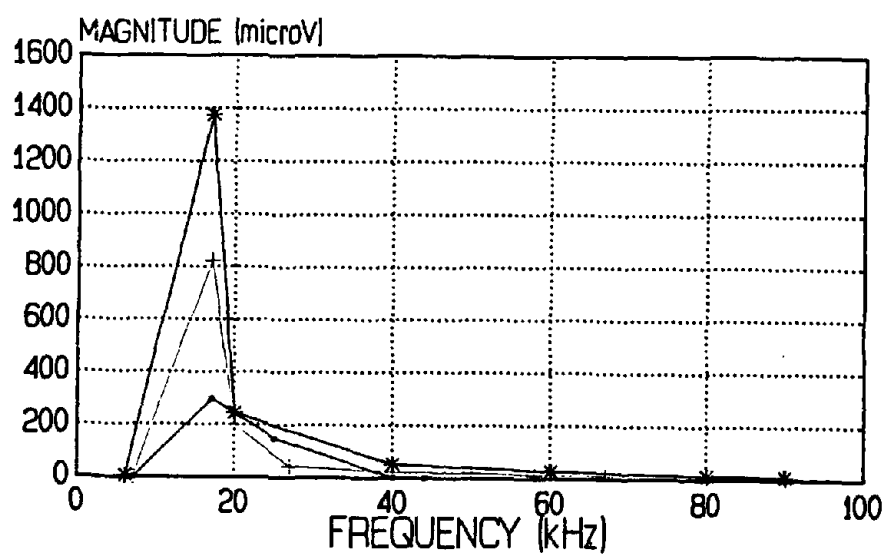


Figure 25. Frequency spectrum with pressure held constant.

Finally, the variation in the magnitude of the 17 kHz component and how it varies with pressure was examined. At a pressure range of 0.06 Torr to 3.7 Torr, the peak 17 kHz signal varied from 16.75 kHz to 17.5 kHz. The plot of this is shown in Figure 26 below.

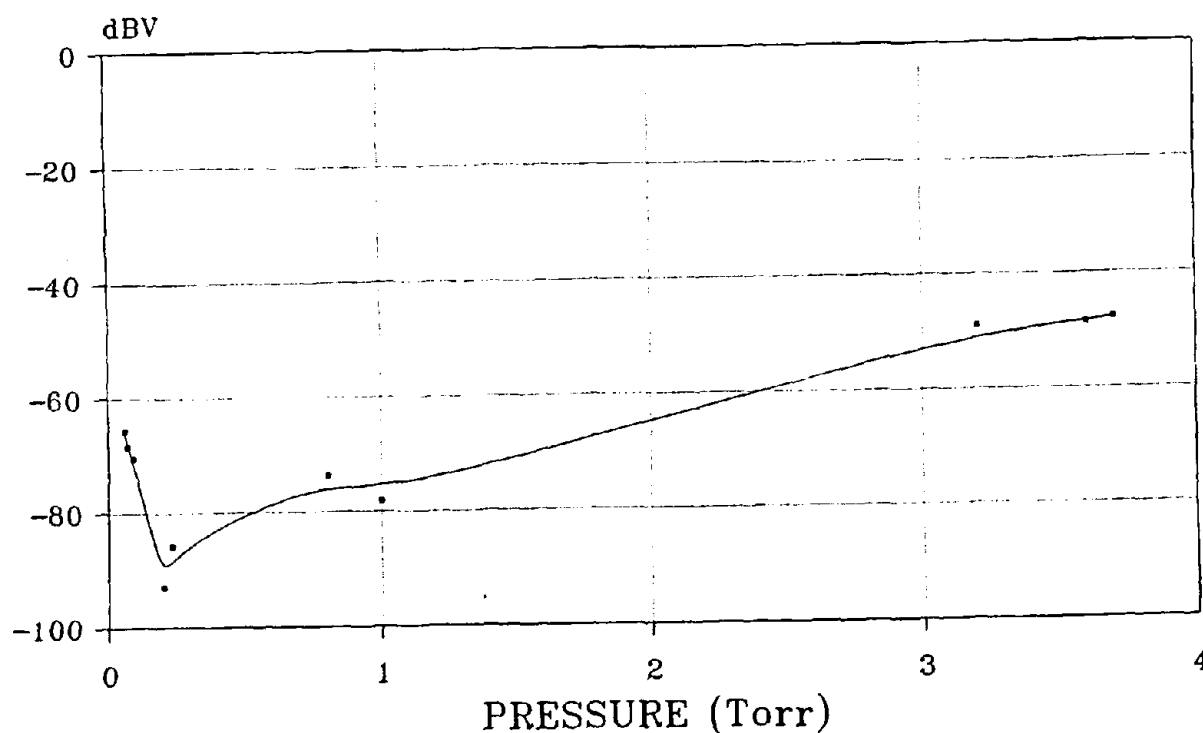


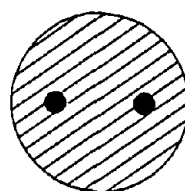
Figure 26. Magnitude of 17 kHz component in corona discharge.

The magnitude of the 17 kHz component of the corona discharge frequency spectrum resembles to some extent the Paschen curve, which corresponds very well to the change in the charge of the corona discharge shown in Figure 7. Fluctuations below 1 Torr, are believed to be due to the difficulty of making the readings at these pressures. The fact that the peak shifted slightly indicates to me that the discharge is probabalistic in nature.

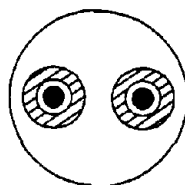
Chapter 5 DATA ANALYSIS AND INTERPRETATION

A. Physical appearance

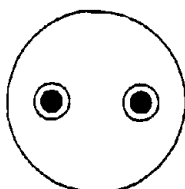
Two items became apparent as a result of these tests. First, we see that a change in the pressure causes a change in the physical appearance in the corona discharge. As shown in the Figure 27 below, we see that for low pressures we have a very even



(a)



(b)



(c)

Figure 27. Changes in the physical appearance of corona discharge with a change in pressure. (a) 668 V, 0.06 Torr (b) 350 V, 1 Torr (c) 453 V, 3.3 Torr

glow in the entire chamber. This glow is very light purple and diffuse. Figure 27 shows a cross section of the vacuum chamber with the two wires side-by-side. As the pressure is increased, the glow becomes less diffuse, and more concentrated around the wires. A pink layer is found immediately around the wire, with a larger purple ring surrounding it. If the pressure is increased even further, only one very tight ring is seen around the wire, which has become very defined and concentrated. It is still purple in color, but white hot spots form along the wires, and red streamers form between the two wires.

If the pressure is left constant and the voltage is reduced, a similar effect is noticed. Two different tests will examine the effects. In the first, the pressure is set at 5.8 Torr. At 342 Volts, corona discharge occurs in the form of a light purple haze in the entire chamber. As the voltage increases, the glow became brighter and distinct layers appear on the wires. At 676 Volts, a purple glow is visible around the wires, with a thin pink layer adjacent to the wires. At 836 Volts, sparking occurs between the wires and at 1000 Volts, a continuous discharge in the form of arcing across the wires begins. The voltage is then decreased and the corona discharge was extinguishes at 302 Volts. In the second test the pressure is set at 7.8 Torr. When the voltage is increased to 624 Volts, corona discharge appears suddenly. At this pressure there is no glow in the chamber, but rather, a bright purple glow which is very limited to the region adjacent to the wires. Hot spots, or white specks jump along both wires and red steamers connect the two wires. The voltage drops to 540 Volts as soon as the discharge occurs, and the pressure in the chamber increases to

8.2 Torr shortly after the discharge begins. As the voltage is increased, the glowing region around the wires increases in diameter and the streamers and hot spots disappear. At 591 Volts, stationary white spots form on the wires. At 750 Volts arcing between the wires is observed. At 800 Volts, streamers from both wires start to appear simultaneously. As the voltage is further increased, these two streamers grow toward each other until they join. When this occurred, the fuse in the circuit blew. At this point, the pressure in the chamber had increased to 10.5 Torr.

Giao and Jordan [46] found that corona discharges at the threshold level appear in the form of streamers or burst pulses. Their work was done on HV transmission lines at atmospheric pressure. They found for corona discharge to exist for parallel conductors the relationship

$$\frac{\alpha}{\tau} \geq 25$$

where tau is the conductor radius and alpha is the distance between the conductors must be satisfied. Giao and Jordan found that as the separation distance between the wires was increased, only the normal glow (shown in Figure 2) would occur. They attributed this phenomenon to the space charge that was developed near the wires. They also mention that the wandering of the hot spots is the result of degassing and deactivating effects of ion bombardment. As they mentioned in their work and I saw in my tests, the streamers formed on the edge of the existing glow

were not related to some disturbance or nonuniformity on the wire surface, and can exist simultaneously with glow discharge.

The tests showed that streamers and burst pulses do not occur simultaneously at low pressure. Rather, steady glow was the first occurrence of corona discharge, bypassing the other two forms that occur at higher pressures. At higher pressures and at CIV, the appearance of the corona discharge would change as the pressure changed. At low pressures the diffuse purple glow was observed, and at higher pressures, the glow would become more concentrated around the wires until, eventually, arcing across the wires caused a short circuit. Also, with the pressure left constant and the voltage increased, the same sort of effect as if the pressure was changing was seen. Corona discharge first appears as a faint purple haze, which would become more constricted and pronounced as the pressure was increased. Streamers did form in this case and eventually flashover and total breakdown occurs.

As was mentioned in Chapter 2, corona discharge occurs when electrons pass through a medium (in this case air) and, as a consequence of their collisions with the molecules or atoms in the medium, cause the emission of photons with wavelengths in the visible spectrum. It should also be noted that the audible corona is the result of the movement of electrons in sufficient number to momentarily displace the air molecules. This displacement results in a mini-vacuum, the collapse of which creates a miniature thunderclap. The movement of the electrons in sufficient quantities constitutes a micro-arc which creates the hertzian waves we can detect as RI [46]. Since the processes here depend on the flow of electrons in the electric field, if we

vary that number by changing the pressure, then we will affect the appearance of the discharge.

The physical change in the appearance of the corona discharge is an outward manifestation of other changes that are taking place in the discharge mechanism. As we have seen, the shape of the pulse and the frequency spectrum, seem to be interrelated in determining the final outcome of the corona discharge.

B. Pulse capture

We saw that as the voltage was increased beyond the CIV (pressure being held constant), the number of bursts per cycle increased. Also, we saw that the number of discharges per cycle at the CIV, increased as the pressure increased. This indicates that the "activity" of the discharge becomes greater as the pressure increases. A similar effect was also seen in the pC versus pressure curve in Chapter 4. The magnitude of the discharge would increase as the pressure increased.

We saw that AC voltage can produce different modes of corona discharge. The particular mode of corona appearance depends upon the polarity, overstressing, and divergence of the distorted region and the space charge. It can also be influenced by the surface properties of the wire and geometrical arrangement. The shape of the corona discharge pulse also changes with a change in pressure. At low pressures, the rise time was much longer than the rise times at higher pressures. This recalls the fact that the faster the rise time, the more high-frequency components must be present. This fact is substantiated by the results of the frequency spectrum tests.

C. Frequency spectrum

The results of these tests were both interesting and unexpected. One of the biggest questions I worked with was, "What is the significance of the 17 kHz component that is so prominent at low pressures?" The first thing investigated was the high-voltage filter designed to take measurements shown in Figure 4. Using the frequency analysis program built into MicroCap II, the frequency response of the filter is shown in Figure 28 below.

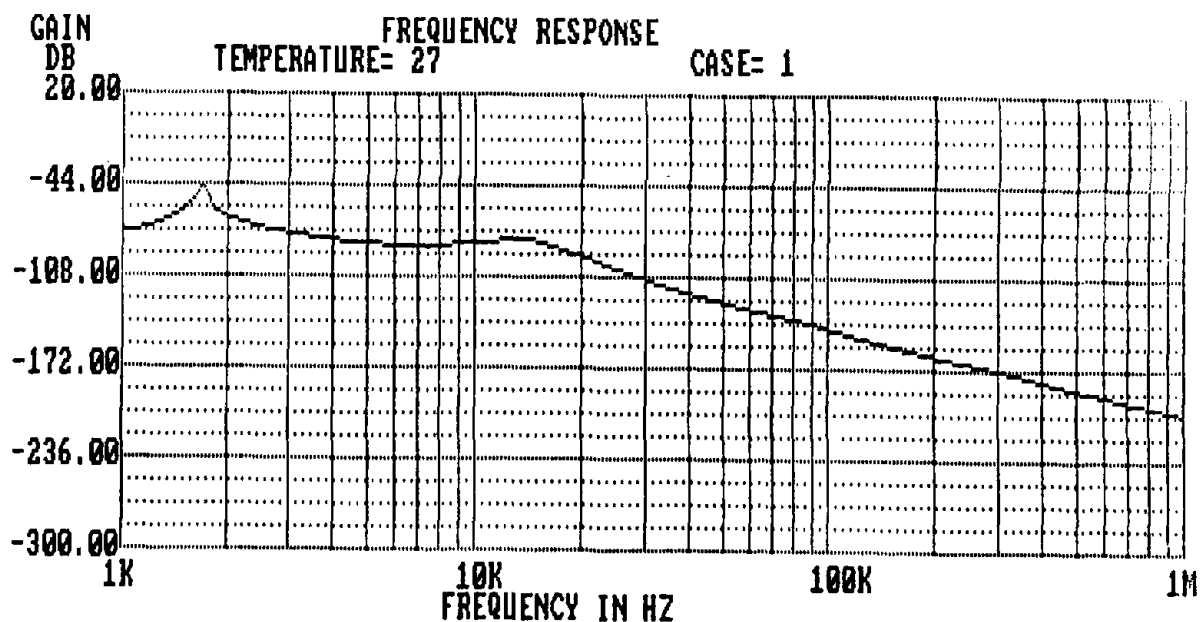


Figure 28. Frequency response of the corona test circuit.

At 17 kHz, the gain is about -70 dB, and the slope is approximately -64 dB/decade for frequencies greater than 17 kHz. The absence of any unusual behavior of the frequency response shown in Figure 28 suggests that the 17 kHz signal is not a

product of the circuit. After examining the circuit component by component, it is concluded that the 17 kHz signal was something inherent in the corona discharge itself and not with the set-up or detection circuit. It may be possible that the frequency is more a function of the arrangement rather than other factors. Giau and Jordan [46] make reference to the repetition rates of the Trichel pulses. They used the term "critical frequencies" to describe this repetition rate, and found that it varied with the electrode geometry, related pulse amplitudes and surface conditions of the conductors.

In order to understand how the frequency changes with pressure and voltage, we need to consider a number of different things.

First, we will look at a test series run on 2 parallel copper wires (No. 12) spaced 7.8 cm apart. In the figure below, we see the voltage-pressure curve generated by this arrangement.

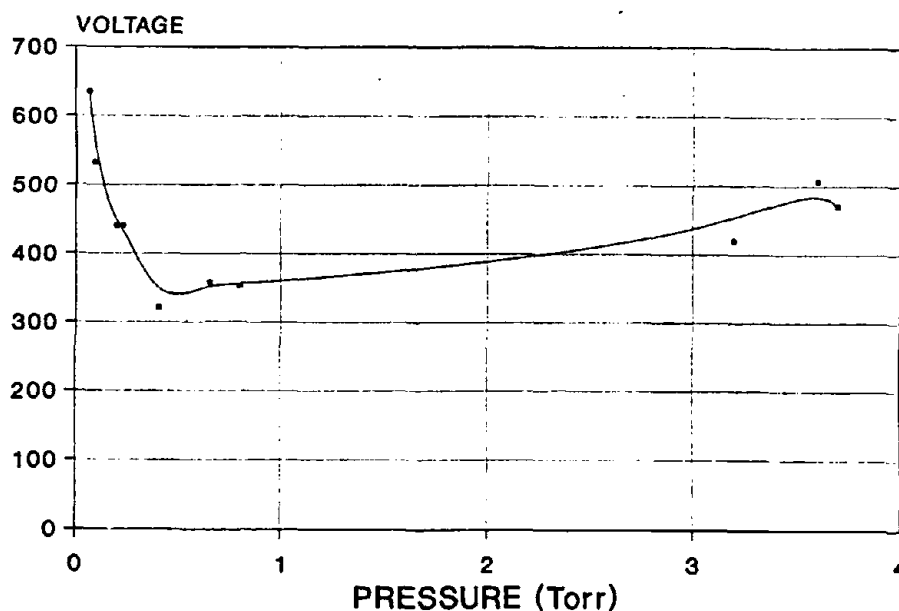


Figure 29. Paschen curve of CIV for parallel wires.

A Paschen minimum occurs at about 350 Volts at 0.4 Torr. While more data for the range from 1 to 3 Torr would be helpful, the data shown suffices for this example. The points were put into a graphics software program and connected with a curve fitting program to show the overall trend. The resulting curve is similar in shape to the classical Paschen curve for parallel plane electrodes.

To examine how the frequency changes with pressure we will examine a typical sample of the spectrum as shown in Figure 30 below. As shown in this figure, we will first take data through the 17 kHz signal as shown by "A" in the figure. This will look to see how the magnitude of this 17 kHz signal changes with the pressure. Then we will look at 3 different dBV levels of the frequency spectrum and see how it changes with pressure at various levels.

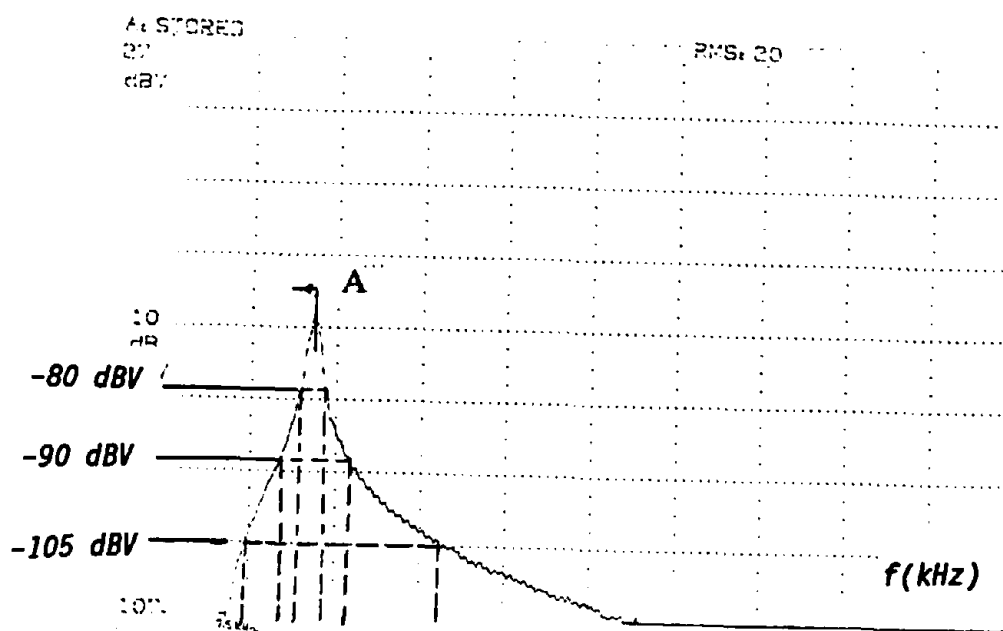


Figure 30. Typical frequency spectrum response.

In Figure 31 below, we see how the magnitude of the 17 kHz signal varies with

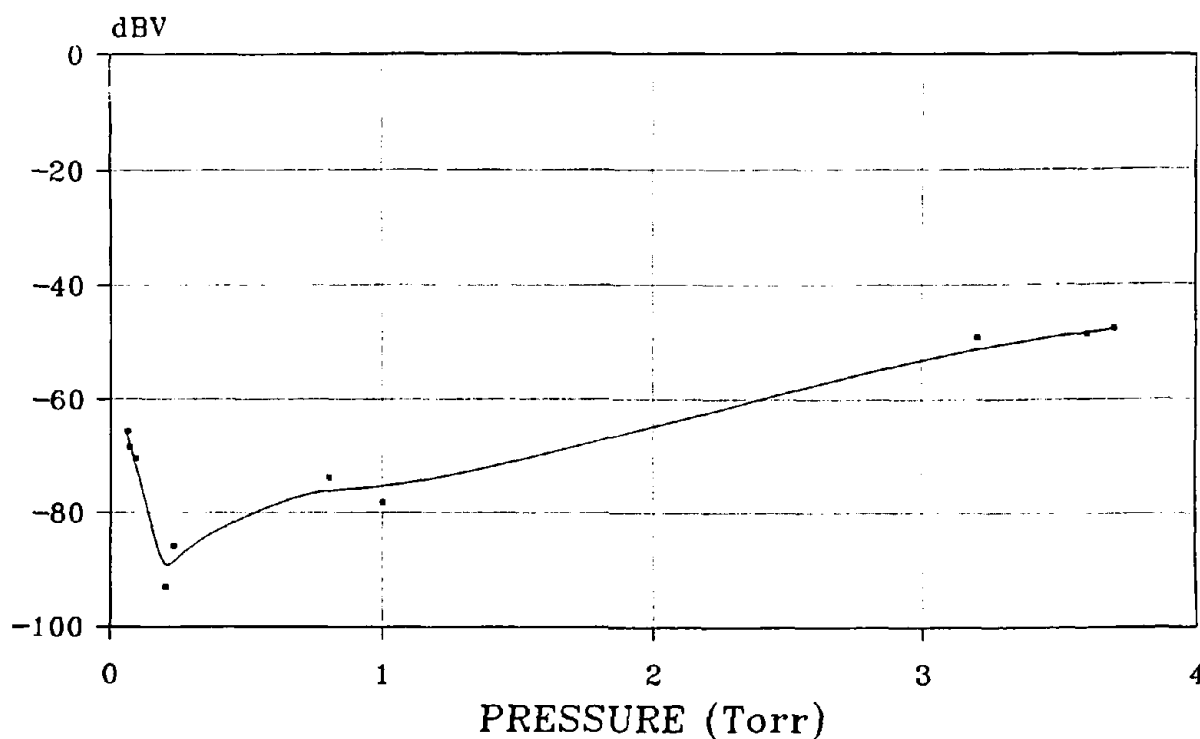


Figure 31. Variation of 17 kHz signal with pressure.

the pressure. Each of these points was taken at the CIV. The trend indicates that the amplitude of the 17 kHz signal also follows a "Paschen-type" curve. There is some error in the region between 0.3 and 1 Torr, but we see good correlation below and above this area. At these pressures, constraints imposed by the available equipment made accurate, quick measurements difficult to obtain. Nevertheless, the results show a similarity to the voltage-pressure curve of Figure 29.

In Figure 32 below, we see the effects of the different dBV levels on the frequency spectrum.

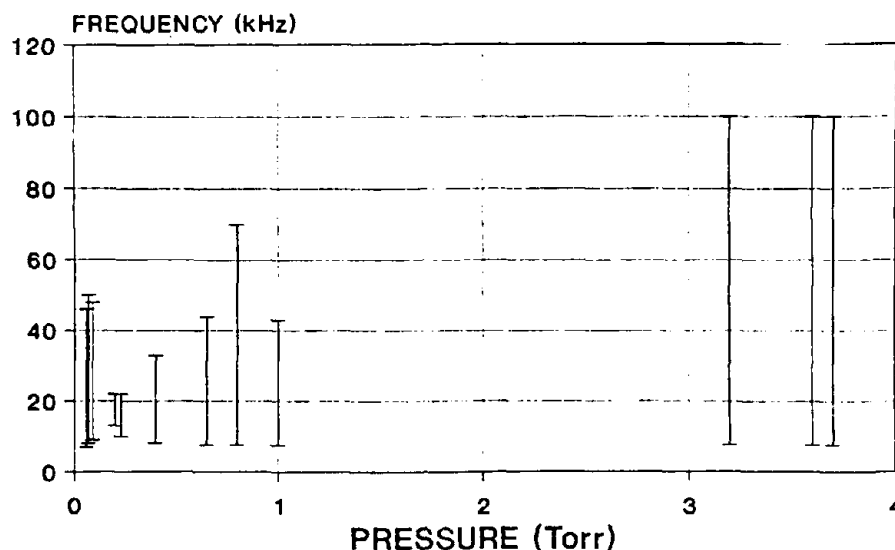


Figure 32. Frequency ranges with pressure for -105 dBV.

Here we see the frequency ranges at the -105 dBV level for the CIV at the various pressures. The frequency-axis shows the high and low frequencies that were present at the -105 dBV level. At this level, we again see a "Paschen-type" response of the frequency spectrum. Notice that in the area of 0.3 Torr (which is close to the minimum of Figure 29) we have a very narrow band of frequencies. This pressure also corresponds to the minimum magnitude of the 17 kHz signal that was shown in Fig. 31.

As the pressure increases, a wider band of frequencies occurs. Again, at 1 Torr, the narrow frequency band in Figure 32 is attributed to measurement error. For the

values above 3 Torr, these points all run from 7.5 kHz to 100 kHz. These values are the limits of the spectrum analyzer in use. Somewhere between 1 and 3 Torr, the frequency band would increase to the maximum of 100 kHz. Also, with a more sensitive machine, we would be able to go past the 100 kHz limit and see how the spectrum is further affected by yet higher pressures.

If we look at the -90 dBV level of the same test points, we have the results shown in Figure 33 below.

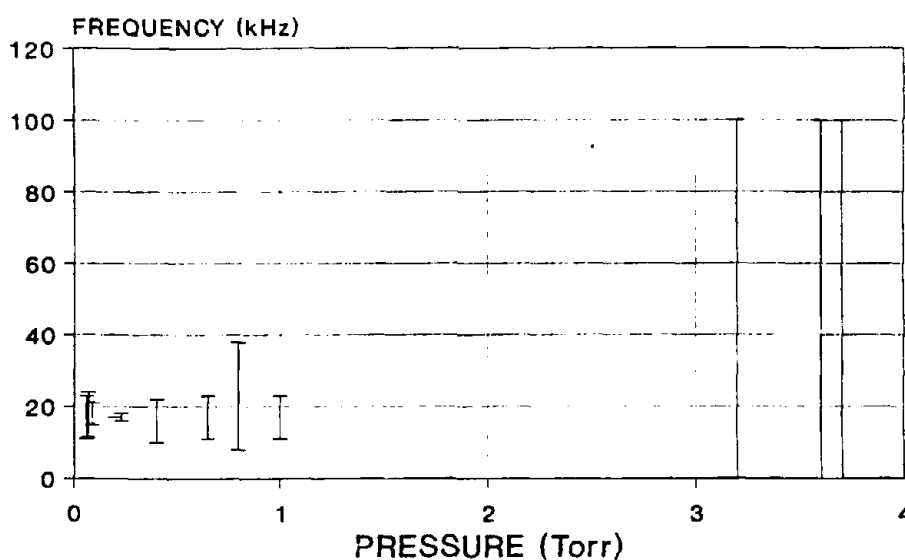


Figure 33. Frequency ranges with pressure at -90 dBV.

Here, the same results are seen; a "Paschen-like" curve that the frequency spectrum follows with a change in the pressure. If we examine one more, this time at -80 dBV, the results shown below.

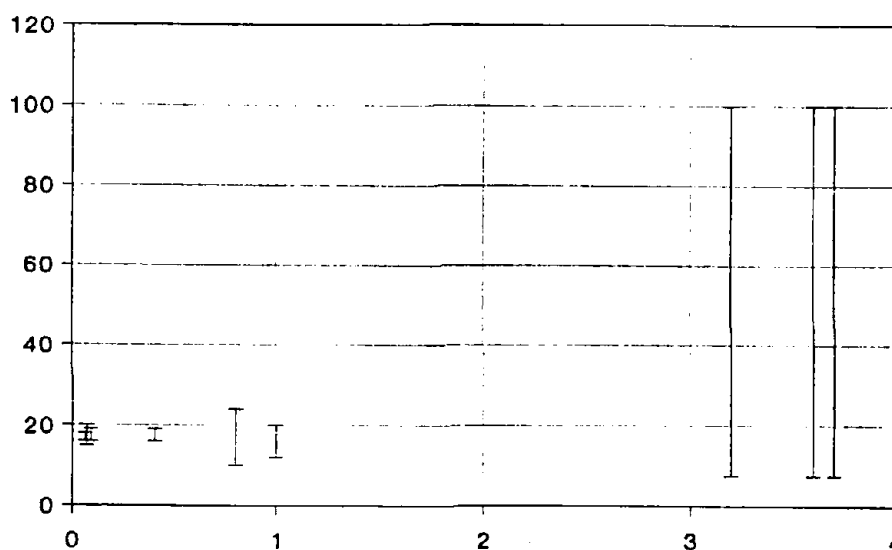


Figure 34. Frequency ranges with pressure for -80 dBV.

Here, a number of the points did not have a magnitude sufficient to show up in this plot. A strong 17 kHz signal was present, but it, and the rest of the spectrum were all below the -80 dBV level needed to show up in this figure.

These tests demonstrated a variation of the classical-Paschen curve in their results. Except for the physical appearance of the corona discharge, which did not demonstrate a similar trait, all other test showed a narrowing or minimum at or very near the Paschen minimum. Other tests showed that the wire size and separation distance did not effect the frequency spectrum that was produced by the corona discharge.

Chapter 6 CONCLUSIONS AND RECOMMENDATIONS

A. Conclusions

This thesis concludes that all corona is not created equally. The magnitude of the corona discharge is not constant. It, like the voltage, follows a Paschen-type curve with a change in pressure. It reaches a minimum at the point where the voltage reaches a minimum, and increases on both sides of that point. The physical appearance of the corona discharge was also shown to change with pressure. At low pressures, it existed as a light purple glow inside the entire chamber. As the pressure increased, the glow became more concentrated and narrowed around the wires. At still higher pressures, the glow was very tight around the wires, hot spots occurred, streamers formed, and eventually, flashover would occur. The fact that the corona discharge changed appearance, indicated that the physical mechanism of the corona discharge was changing. This change in the appearance may be due in part to the changing frequency spectrum of the discharge current. However, it is more likely due to changes in the mean free path as the voltages alters the electric field between the wires.

The pulses of the corona discharge, superimposed on the 60 Hz source voltage were next examined. As the pressure was increased, the frequency of the discharges also increased. A study of the corona discharge pulse shape shows that the low pressure corona discharge has lower frequency components than the higher pressure pulses. Using the spectrum analyzer, we looked at the frequency spectrum of the corona discharge. A direct correlation between this and the pulse capture studies

can be seen. At low pressures, the frequency spectrum is different than the frequency spectrum produced at high pressures. The low pressure spectrum produced a very strong 17 kHz signal that became predominate in the lower pressure ranges. The peak magnitude of this 17 kHz signal follows a Paschen-type curve as shown in Chapter 5. Looking at the frequency spread at different levels, we see that the range of frequencies narrows at the Paschen minimum, and grows again as the pressure increases. This phenomenon becomes very important in the area of corona discharge detection. As shown in Figure 35 below, we see the three different band settings of the partial discharge detector that was used in this research.

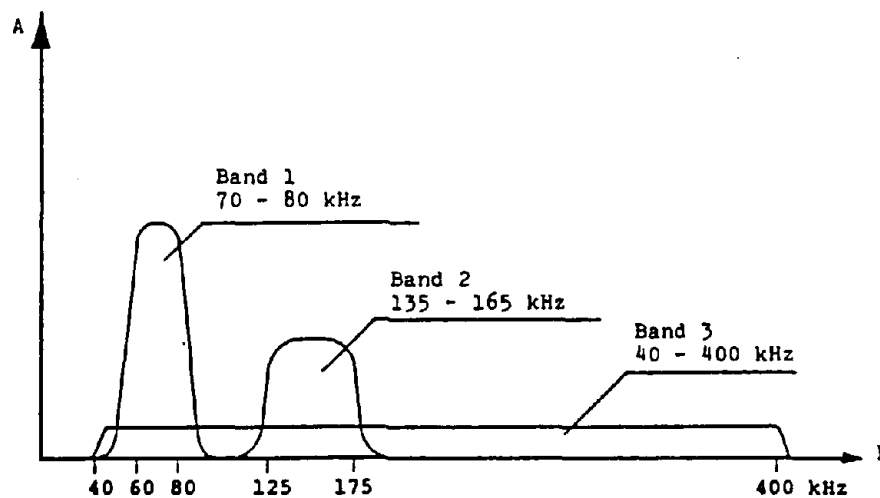


Figure 35. Detection bands for partial discharge detector.

This shows that the lowest frequency signal this detector will pick up is 40 kHz. If the corona discharge is at such a low pressure so that all the frequency components fall below 40 kHz, there will be no detection of the corona discharge. Proper detection requires that the machine be able to function at all pressures, and with a greater frequency band.

B. Recommendations

This section includes recommendations for additional work that needs to be done in this area to further understand the corona discharge process. Most of these recommendations include areas that were not covered, either because of a lack of money, or a lack of time. However, these items would be very useful for continued research to increase the knowledge base of this area.

In the paper by Karady *et al.* [3], results of CIV with and without insulation were presented. These tests were done with bare wires, and it would be beneficial to see the effect that insulation has on the frequency spectrum characteristics of the corona discharge. Based on the literature review, one would assume that the CIV would be higher, but the spectrum would need to be studied for changes.

Giao and Jordan [46] found some very interesting results with respect to the "critical frequency" of the discharge. They found that geometry played an important role in this area. It would be useful to study the effect on the frequency spectrum using different arrangements. For example, does a strong 17 kHz signal manifest itself in the corona discharge of parallel plates, two spheres, or perhaps a point to

plane arrangement? This would lend to a better understanding of the significance of the 17 kHz component.

The tests used bare copper wires only. The results of aluminum, steel and gold conductors would also be helpful in understanding this phenomenon. Since these tests were conducted in room air only, the variations caused by different gases in the vacuum chamber would also be of interest for testing.

The change in the pressure in the tests to examine the physical appearance need to be examined further. This could be done by monitoring the heat generated by the corona discharge at different pressures and/or voltages. Since the charge (pC) level of the corona discharge was not constant, it would be useful to study the affect of aging on the conductors at low pressure. This would be of great worth to designers of high altitude aircraft.

The pulse capture tests need to be repeated to better understand this phenomenon. These tests need to be carried out from the low pressure range, up to and including atmospheric pressure. My tests were limited to pressures below 10 Torr, and further tests need to be done at 760 Torr, and possibly higher.

The literature on corona discharge often refers to discharge lasers. It would be useful to see if the frequency of the discharge of the lasers is affected by pressure.

REFERENCES

- [1] F. Llewellyn-Jones, *The Glow Discharge*. New York: Wiley, 1966, pp. 1-3.
- [2] L. B. Gordon, "High voltage breakdown in the space environment," presented at IECEC, Denver, CO, 1988, paper 889478.
- [3] G. G. Karady, M. D. Sirkis, and L. Liu, "Investigation of high altitude corona initiation voltage," to be published.
- [4] Electrical Power Research Institute, *Transmission Line Reference Book, 345 kV and Above*. Palo Alto: EPRI, 1987, pp. 169-171.
- [5] M. Goldman and A. Goldman, *Gaseous Electronics, Vol. 1, Electrical Discharges*. New York: Academic Press, 1978, pp. 219-225.
- [6] J. S. Townsend, *Electricity in Gases*. Oxford: Clarendon Press, 1915, pp. 79-82.
- [7] J. M. Meek and J. D. Craggs, *Electrical Breakdown of Gases*. Oxford: Clarendon Press, 1953, pp. 80-83.
- [8] S.C. Brown, *Introduction to Electrical Discharges in Gases*. New York: Wiley, 1966, pp. 211-215.
- [9] A. M. Howatson, *An Introduction to Gas Discharges*. Oxford: Pergamon Press, 1965, pp. 55-57.
- [10] Q. Vuhuu and R.P. Comsa, "Influence of gap length on wire-plane corona," *IEEE Trans. Power Appr. and Sys.*, vol. 88, pp. 1462-1475, 1969.
- [11] F. Paschen, "Ueber die zum funkenuebergang in luft, wasserstoff und kohlensaeure bei verschiedenen drucken erforderliche potentialdifferenz," *Ann. Phys. Chem.*, vol. 37, pp. 69-96, 1889.
- [12] L. J. Berberich, G. L. Moses, A. M. Stiles, and C. G. Veinott, "Effects of altitude on electrical breakdown and flashover of aircraft insulation," *Trans. AIEE*, vol. 63, pp. 345-354, 1944.
- [13] W. R. Wilson, "Corona in aircraft electric systems as a function of altitude," *Trans. AIEE*, vol. 63, pp. 189-194, 1944.
- [14] W. W. Pendleton, "High altitude flashover and corona correction on small ceramic bushings," *Trans. AIEE*, pp. 1324-1330, 1947.

- [15] W. J. Linder and H. L. Steele, "Estimating voltage breakdown performance of high altitude antennas," presented at Wescon Conference, San Francisco, CA, 1959.
- [16] W. T. Starr, "High altitude flashover and corona problems, part 1," *ElectroTechnology*, pp. 124-127, May 1962.
- [17] F. W. Paul and D. R. Burrowbridge, "Prevention of electrical breakdown in spacecraft," *IEEE Trans. Elec. Ins.*, vol. 6, pp. 114-123, 1971.
- [18] NASA/JCS, "Aerospace corona bibliography and survey," *publication number D180-14867-1*, October 1972.
- [19] R. J. VanBrunt and W. E. Anderson, "Bibliography of data on electrical breakdown in gases," *Dept. of Energy Pub. No. NCS-TN-1195*, April 1984.
- [20] C. Gary, B. P. Hutzler, and J. P. Schmitt, "Peek's law generalization, application to various field configurations," presented at IEEE PES Conference, San Francisco, CA, 1972.
- [21] L. Chong-hui and L. Zheng-xiang, "The influence of altitude on corona starting voltages," presented at the 6th International Symposium on High Voltage Engineering, New Orleans, LA, 1989, paper 22.10.
- [22] D. He and D. R. Hall, "Frequency dependence in RF discharge excited waveguide CO2 lasers," *IEEE J. Quantum Electron.*, vol. QE-20, pp. 509-514, 1984.
- [23] S. Suganomata, I. Ishikawa, S. Ohmoto, T. Akitsu, and Y. Saito, "Spatiotemporal variation of light emission from SF6 parallel-plate discharge at frequencies of 100 and 500 kHz," *Japan. J. Appl. Phys.*, vol. 28, pp. 2265-2266, 1989.
- [24] N. Sato and S. C. Haydon, "Time-resolved observations of RF corona in air and nitrogen," *J. Phys. D:Appl. Phys.*, vol. 17, pp. 2009-2021, 1984.
- [25] I. Ishikawa, K. Koike, T. Akitsu, S. Suganomata, and H. Matsuzawa, "Detection technique of negative ions by photodetachment in SF6 low-frequency discharge," *Japan. J. Appl. Phys.*, vol. 29, pp. 767-768, 1990.
- [26] M. C. Damas and R. T. Robiscoe, "Detection of radio-frequency signals emitted by an arc discharge," *J. Appl. Phys.*, vol. 64, pp. 566-574, 1988.

- [27] R. J. Seeboek and W. E. Koehler, "Temporal intensity modulation of spectral lines in a low-frequency discharge in argon," *J. Appl. Phys.*, vol. 64, pp. 3855-3862, 1988.
- [28] S. Ballantine, "Fluctuation noise due to collision ionization in electronic amplifier tubes," *Physics*, vol. 4, pp. 294-306, 1933.
- [29] I. Ishikawa and S. Suganomata, "Frequency shift of positive column oscillation due to external electric field in SF₆ gas glow discharge," *Japan. J. Appl. Phys.*, vol. 15, pp. 1855-1856, 1976.
- [30] I. Ishikawa, M. Matsumoto, and S. Suganomata, "Ionisation waves in low pressure SF₆ gas," *J. Phys. D:Appl. Phys.*, vol. 17, pp. 85-97, 1984.
- [31] S. Suganomata, I. Ishikawa, Y. Matsuoka, and M. Matsumoto, "Nonlinear interaction of externally excited waves with spontaneous ionisation waves in SF₆ gas," *J. Phys. D:Appl. Phys.*, vol. 17, pp. 301-305, 1984.
- [32] N. Sato and S. C. Haydon, "Nanosecond time-resolved spectroscopic investigations of RF corona with high spatial resolution," *J. Phys. D:Appl. Phys.*, vol. 17, pp. 2023-2036, 1984.
- [33] D. B. Ogle and G. A. Woolsey, "Diffuse and constricted glow discharges in SF₆," *J. Phys. D:Appl. Phys.*, vol. 20, pp. 453-461, 1987.
- [34] S. Suganomata, I. Ishikawa, M. Gyoten, and M. Matsumoto, "Transient current oscillation in a low frequency glow discharge of CF₄ gas," *Phys. Letters A*, vol. 133, pp. 242-244, 1988.
- [35] M. Beyer, H. Borsi, and O. Cachay, "Some aspects about basic investigations of acoustic partial discharge (PD) detection and location in cast epoxy resin coils," presented at the 6th International Symposium on High voltage engineering, New Orleans, LA, 1989, paper 22.20.
- [36] R. J. Van Brunt and D. Leep, "Characterization of point-plane corona pulses in SF₆," *J. Appl. Phys.*, vol. 52, pp. 6588-6600, 1981.
- [37] R. J. Van Brunt, S. H. Hilten, and D. P. Silver, *Gaseous Dielectrics II*. New York: Pergamon Press, 1980, pp. 303-311.
- [38] R. J. Van Brunt, "Effects of H₂O on behavior of SF₆ corona," Proc. 1982 IEE Conf. on Gas Discharges and Their Applications, U.K.

- [39] R. Bartnikas, "Corona pulse counting and pulse height analysis techniques," *Engineering Dielectrics, Corona Measurement and Interpretations*, vol. I, ASTM: Philadelphia, pp. 285-326, 1979.
- [40] A. A. Al-Arainy, N. H. Malik, and M. K. Al-Bahloul, "Statistical variation of ac corona pulse amplitudes in point-to-plane air gaps," *IEEE Trans. Elec. Ins.*, vol. 24, pp. 681-687, 1989.
- [41] N. H. Malik and A. A. Al-Arainy, "EMI characteristics of distribution lines located in desert lands," *IEEE Trans. Electrmag. Comp.*, vol. 31, pp. 273-279, 1989.
- [42] J. A. Cross, "An analysis of the current in a point-to-plane corona discharge and the effect of a back-ionising layer on the plane," *J. Phys. D:Appl. Phys.*, vol. 18, pp. 2463-2471, 1985.
- [43] H. W. Bandel, "Point-to-plane corona in dry air," *Phys. Review*, vol. 84, pp. 92-99, 1951.
- [44] T. M. Bilodeau, W. G. Dunbar, and W. J. Sarjeant, "High-voltage and partial discharge testing techniques for space power systems," *IEEE Elec. Ins. Mag.*, vol. 5, pp. 12-21, 1989.
- [45] L. B. Loeb, *Fundamental Processes of Electrical Discharge in Gases*. New York: Wiley, 1947, pp. 560-567.
- [46] T. N. Giaio and J. B. Jordan, "Modes of corona discharges in air," *IEEE Trans. Power Appr. and Sys.*, vol. 87, pp. 1207-1215, 1968.

APPENDIX A
HP 3561A
TECHNICAL DATA

Specifications describe the instrument's warranted performance. Supplemental characteristics give typical, but non-warranted, performance specifications. Supplemental characteristics are denoted as 'typical,' 'nominal,' or 'approximately.'

Frequency and Time

Measurement Modes:

Narrowband: 125 μ Hz to 100,000 Hz frequency range.

Phase: Phase spectrum is available with or without triggering. When triggered, phase can be referenced to the trigger. (See AMPLITUDE and INPUT.)

1/3 Octave

Full Octave

Time Capture: Time record can be extended from 1k to 40k samples of continuous input data. Up to 40x zoom expansion factor can be applied to this data with variable center frequency.

External Sampling: Input sample rate can be externally controlled up to 256 kHz. TTL compatible sample rate input on rear panel. (Note: Some specs may be degraded in external sample mode).

Accuracy:

Frequency Accuracy: $\pm 0.003\%$ of frequency reading

Resolution:

Frequency Resolution: Span/400

Spans:

	Zoom	Baseband
# spans available	43	52
min span	0.25 Hz	0.01 Hz
max span	100 kHz	100 kHz
time record length	400/span	400/span
resolution	span/400	span/400

Measurement Windows:

Window Types: Flat Top, Hanning, Uniform, Exponential

Window Parameters:

	Flat	Hann	Uniform
Noise Equiv.	0.955	0.375	0.25
BW (% of span)			
3dB BW	0.90	6.37	0.25
(% of span)			
Shape factor	2.6	5.1	7.15
(60dB BW/3dB BW)			

Typical Real-Time Bandwidth:

Operating mode	Real-time bandwidth	Spectra/sec
HP-1B transfer	650 Hz	1.6
Single display	3 kHz	7.5
Fast averaging	7.5 kHz	20

Amplitude and Input

Amplitude:

Input Range: The calibrated input range is 27 dBV (+22.4 V) to -51 dBV (3 mV) maximum input level (single tone RMS). Range is adjustable in 1 dB (10%) increments.

Autorange: The optimum input range is automatically selected prior to processing. This feature can be deactivated.

Amplitude Overload/Underload:

Overload occurs when the input level exceeds input range by nominally 1.0 dB or 10%. Overload measurements can be automatically rejected during averaging. The HALF range indicator lights when input signal is within 6 dB of full scale.

Dynamic Range: Distortion, spurious and alias products ≥ 80 dB below input range

DC Response: (With Auto-Cal on)

+27 dBV to -35 dBV:

>30 dB below input range

-36 dBV to -51 dBV:

>20 dB below input range

Amplitude Marker Resolution:

Log: 0.01 dB

Linear: 4 digits

Amplitude Accuracy:

Full Scale Accuracy at calculated frequency points. Overall accuracy is the sum of absolute accuracy, window flatness and noise level.

Absolute Accuracy:

± 0.15 dB $\pm 0.015\%$ of input range:

+27 dBV to -40 dBV

± 0.25 dB $\pm 0.025\%$ of input range:

-41 dBV to -51 dBV

Window flatness:

Flat top: +0, -0.01 dB

Hanning: +0, -1.5 dB

Uniform: +0, -4.0 dB

Noise Level: Flat top filter, 50 Ω source

impedance, 20 Hz to 1 kHz (1 kHz span)

< -131 dBV (-141 dBV/ $\sqrt{\text{Hz}}$)

2 kHz to 100 kHz (100 kHz span)

< -120 dBV (-150 dBV/ $\sqrt{\text{Hz}}$)

Phase:

Phase Marker Resolution: 0.1 degree

Phase Accuracy: $\pm 2^\circ$ from dc to 10 kHz; $\pm 10^\circ$ from 10 kHz to 100 kHz (signals no more than 40 dB below full range).

Input:

Input Impedance: 1 M Ω $\pm 5\%$ shunted by 95 pF maximum. Floating ground

to case capacitance: <0.25 μ F

DC Isolation: Input low may be connected to chassis ground or floated up to 30 volts RMS (42 Vpk).

Input Coupling: Ac or dc coupled.

Low frequency 3 dB roll off < 1.0 Hz for ac.

Anti-Alias Filter Roll-Off: Nominally 130 dB/octave; cut-off frequency at 105 kHz nominally.

A-Weight Filter: The hardware A-weight input filter conforms to ANSI Standard S1.4-1971.(R1976)

ICP Current: Nominal 4 mA current

source provided on input BNC

connector. Compatible with integrated circuit piezoelectric accelerometers.

Open circuit voltage is 24 volts nominal.

HP 3561A Specifications

Octave Analysis

The measurement is made in synthesized 1/3 or full (1/1) octave bands. Filter bandwidth, center frequency and bandshape meet specifications of ANSI S1.11-1966(R1976). MIL-STD-740-2 is also met provided at least six averages are used.

	# Bands Available	# Band Displayed
1/3	51	33
1/1	17	11

1/3 and 1/1 Octave Analysis

Parameters:

	Band Center Frequency Range	Data Collection Time	Band #'s Displayed
1/3 Octave	50 Hz to 80 kHz	0.4 sec	17 to 49
	25 Hz to 40 kHz	0.8 sec	14 to 46
	12.5 Hz to 20 kHz	1.6 sec	11 to 43
	6.3 Hz to 10 kHz	3.2 sec	8 to 40
	3.15 Hz to 5 kHz	6.4 sec	5 to 37
	1.6 Hz to 2.2 kHz	12.8 sec	2 to 34
	0.8 Hz to 1.25 kHz	25.6 sec	-1 to 31
1/1 Octave	63 Hz to 63 kHz	0.4 sec	18 to 48
	31.5 Hz to 31.5 kHz	0.8 sec	15 to 45
	16 Hz to 16 kHz	1.6 sec	12 to 42
	8 Hz to 8 kHz	3.2 sec	9 to 39
	4 Hz to 4 kHz	6.4 sec	6 to 36
	2 Hz to 2 kHz	12.8 sec	3 to 33
	1 Hz to 1 kHz	25.6 sec	0 to 30

Computation Time: 1/3 octave and 1/1 octave computation is made in less than 0.80 seconds.

Trigger

Trigger Modes:

Free Run, external, internal, input, source, HP-IB

Trigger Arm:

Auto arm, manual arm

Trigger Level:

0 to 110% of full range. Positive and negative levels and slopes.

Trigger Delay:

Pre-Trigger: The measurement can be based on input data from 1/1024 to 9 time records before trigger conditions have been met, with resolution of 1/1024 of a record. Time capture mode can be used for pre-trigger delays of up to 40 records.

Post-Trigger: The measurement is initiated from 1/1024 to 1023 time records after trigger conditions have been met. Resolution is 1/1024 of a record.

Measurement Averaging

Averaging Types:

RMS, peak hold, RMS exponential weighting, time

Number of Averages: 1 to 16,383.

Average Control:

Start, pause/continue, overload reject, fast display, normal display, repeat display

Source

Description:

Band limited, band translated pseudo random, random, impulse or TTL "sync" signals are available on the rear panel. Impulse produces nominal 2 V peak into 50 Ω , with no attenuation.

Impedance:

50 ± 5 ohms.

Level and Accuracy

Baseband All spans* 0.7 V rms $\pm 10\%$

Zoom All spans 0.5 V rms $\pm 15\%$

*Random Source in 0-100 kHz span has level accuracy of $\pm 20\%$.

Flatness:

		Periodic	Random**
Baseband	0-50 kHz	± 0.7 dB	± 0.7 dB
	0-100 kHz	± 0.8 dB	± 1.6 dB
zoom	all spans	± 2.0 dB	± 2.0 dB

**Random Source flatness approaches these specs as number of RMS averages increases.

Note: All zoom flatness specs are valid if center frequency $> 0.7 \times$ span

Attenuation:

(nominal 1.5 dB steps) max attenuation

pseudo-random, random 40.5 dB
impulse 30 dB

Display

Description:

Magnitude, Phase, Time and Math traces may be selected.

Horizontal units: Hz, seconds, RPM, and orders with linear or logarithmic spacing.

Vertical units: volts, volts², dBV, dBm (selectable R), and user-defined units.

Magnitude:

Log: 0.5 to 40 dB/division. Units of dBV, dB relative, dBm (user-defined impedance) and dBm (user-defined impedance) are provided.

Linear: Constant volts/division, milliwatts/division, or user-defined units/division.

Frequency:

Display Range: 115 kHz (accuracy above 100 kHz not specified).

Phase:

Resolution: 0.1 degree with marker

Display Range: ± 240 degrees about user-definable center reference. (± 320 degrees)

Time:

Resolution = Record Length (sec)/400

Display Range: $\pm 110\%$ of input range.

Math:

Arithmetic operations can be performed on new and recalled spectra. Addition, subtraction, multiplication, division, single and double integration, differentiation and user-definable constants are provided. 1/BW is provided for PSD computations.

Format:

Single, front-back, upper-lower, map

Scale:

Linear or log magnitude scales; user-definable full scale, dB/div, and degrees/div; center scale definable in time or phase traces; auto-scale.

Internal Memory

	Traces + States (non-volatile)	Time Buffer (volatile)
Standard	2 traces + 6 states	40 time records
Option 001	traces + states + (1 + 2 x time capture records) = 127	40 time records

Marker**Single:**

X and Y axis, MKR → Peak, MKR → Center Frequency, MKR → Full Scale, Peak-track, Relative markers.

Band Pass:**Harmonic:**

Up to 20 harmonics, total harmonic distortion (THD).

Sideband:

Up to 10 modulation sidebands.
Carrier frequency is user definable.
The ratio of sideband to carrier power is displayed.

Marker Resolution:

log: 0.01 dB

linear: 4 digits

phase: 0.1 degrees

Plot

Controls HP-GL compatible digital plotters and raster graphics printers directly. Replicates display contents. "MARKER plot" allows marker position and amplitude to be annotated on plots at user-definable locations.

General**Specifications apply when.**

Warm-up time: None with AUTO-CAL enabled, or 30 minutes without AUTO-CAL enabled.

Within 5° C and 2 hrs of last internal calibration.

Ambient temperature: 0° to 55° C.

Relative Humidity: < 95% at 40° C.

Altitude: < 4570m (15,000 ft.)

Storage:

Temperature: -40° to +75° C.

Altitude: < 15,240m (50,000 ft.)

Power:

100/120 VAC +6% -14%, 48-440 Hz

220/240 VAC +5% -10%, 48-66 Hz

150 VA maximum

Weight:

15 kg (33 lbs) net

21.5 kg (47.5 lbs) shipping

Dimensions: Without handle:

197mm (7.8") high

335mm (13.2") wide

595mm (23.4") deep

HP-IB:

Implementation of IEEE Std 488-1978
SH1 AH1 T5 TE0 L4 LE0 SR1 RL1
PP0 DC1 DT1 C0

Accessories Included: Front (bail) handle, pouch, front cover, operating and service manuals.

Ordering Information.

HP 3561A Dynamic Signal Analyzer

Opt. 001: Extended Non-volatile Memory

Field upgrade for opt. 001:

03561-68742

Opt. 910: Extra Op. and Svc. Manuals

Accessories:

Transit case for 3561A:

HP #9211-6445

Rack Adapter for HP 3561A:

HP #10491B

Accelerometers:

HP 35200A:

ICP accelerometer for general vibration measurements

HP 35201A:

ICP accelerometer for machinery vibration measurements

Microphones and accessories:

HP 35220A:

1/2" free field, standard sensitivity microphone

HP 35221A:

1/2" free field, high sensitivity microphone

HP 35222A:

1/2" pressure, standard sensitivity microphone

HP 35223A:

1/2" pressure, high sensitivity microphone

HP 35224A:

Microphone pre-amplifier

HP 34228A:

Power supply. (Supports 2 pre-amps.)

HP 34229A:

Microphone calibrator

DISTRIBUTION

WL/SUL/HO, KAFB, NM
AFCSA/SAMI, Washington, DC
AUL/LSE, Maxwell AFB, AL
DTIC/FDAC, Alexandria, VA
Arizona State University, Tempe, AZ
Hellenic Aerospace Industries, Westlake Village, CA
HV Insulation Packaging, Bellevue, WA
McDonnell Aircraft, St Louis, MO
NASA Lewis Research Center, Cleveland, OH
Reynolds Industries Inc, Los Angeles, CA
Unisys Corporation, Salt Lake City, UT
WRDC/POOC, Wright-Patterson AFB, OH
Official Record Copy
PL/WSBOF, KAFB, NM 87117-6008